The Molecular Basis Underlying Heme Biosynthesis Dysfunction and Disease Originating from C-Terminal Mutations in Aminolevulinic Acid Synthase

By

Jessica Lynn Taylor

Dissertation

Submitted to the Faculty of the

Graduate School of Vanderbilt University

in partial fulfillment of the requirements

for the degree of

DOCTOR OF PHILOSOPHY

in

Biochemistry

August 9, 2024

Nashville, Tennessee

Approved:

Charles Sanders, Ph.D.

Manuel Ascano, Ph.D.

David Cortez, Ph.D.

TM Iverson, Ph.D.

Breann Brown, Ph.D.

To my daughter, Rose

I am so happy you are here.

ACKNOWLEDGMENTS

I would like to thank all former and current members of the Brown laboratory for enduring, supporting, and encouraging me in my scientific pursuits throughout my Ph.D. A special thank you to Nicolle Serrano, Iva Chitraker, and Jenny Tran. It was the day-to-day moments that got me through the weeks, the months, and the years of my Ph.D. I am especially indebted to Dr. Iva Chitraker who took the time to parse through mounds of confusing data with me in a dark and difficult time during my graduate career. This, along with countless other moments, reinvigorated my scientific spark and curiosity and certainly allowed me to finish this Ph.D. in a positive scientific light. I am forever grateful to her for her selflessness and willingness to care about a project that was not even hers. She inspires me and reminds me to stay curious and patient.

Thank you to the core group of friends that I made during my time in graduate school: Brett Nabit, Sam Lisy, Serena Sweet, Sirena Tran, Lindsey Guerin, Cayla Ontko, and Michelle Piazzo. From Friendsgivings, potluck brunches, and goat farms, I will cherish the happy times we spent together as we navigated the hardest thing we have ever done.

Thank you to my husband, Michael Moore, for always believing in me. Your unwavering confidence in me made me believe in myself on the extremely difficult days. Not only that, but you always reminded me of the love and life that exists beyond graduate school, and I know that I may not have been able to persevere without that reprieve. You have been inspirational in many ways – intellectually, physically, and emotionally. Your work ethic has always inspired and amazed me, and I am thankful for all the long nights that we got to share together, even if we were working. Thank you for being my partner and best friend.

Thank you to my committee, Chuck Sanders, Manny Ascano, Dave Cortez, Tina Iverson, and Breann Brown. Your insight, knowledge, and commitment to the success of my project helped me to see aspects of my project that I could not or did not want to see. You upheld outstanding scientific rigor and challenged me at every committee meeting to always consider an additional outcome that I, once again, had not considered. You never doubted my abilities, and you always guided me with kindness and wisdom that can only come from seasoned scientists. Thank you.

Thank you to anyone who played a role in my life during graduate school, big or small. From saying hello in the hallway to assisting with a new technique, I truly believe the culmination of these interactions were the best part of graduate school.

Thank you to my former mentor, Dr. Xiahuoa Jiang, who mentored me in her laboratory as a master's student and encouraged me to pursue a Ph.D. Your belief and trust in me instilled the confidence that I needed to complete a Ph.D. Even today, you believe in me to accomplish and excel in any step I take. Thank you for opening my eyes to research and trusting me to accomplish a challenging new project in your lab. I am forever grateful for the hard and soft skills I learned during that time.

TABLE OF CONTENTS

LIST OF TABLES

LIST OF FIGURES

CHAPTER 1

Introduction

1.1 The Versatility and Vitality of Heme Across Life Forms

Heme is a critical molecule involved in essential processes across domains of life (Ferreira, 2013; Layer, 2021). Heme performs a variety of functions including oxygen transport, electron transfer, signal transduction, and gene regulation among prokaryotes and eukaryotes (Chiabrando, Mercurio, & Tolosano, 2014; Ferreira, 2013; Layer, 2021; Munro, Girvan, McLean, Cheesman, & Leys, 2009). Structurally, heme belongs to the metalated porphyrin group of heterocyclic compounds consisting of four pyrrole rings coordinating a central iron atom (**Figure 1**) (Layer, 2020, 2021). Other molecules in this family are chlorophylls, cobalamin (vitamin B_{12}), siroheme, and coenzyme F_{430} (Ferreira, 2013; Wintrobe & Greer, 2004). Although the central metal ion in these molecules differ from heme, the metalated porphyrin structure promotes the same remarkable diversity of biochemical processes (Ferreira, 2013; Rich, 2012).

There are various types of heme that are differentiated by the structure and substituents of their porphyrin ring (Rich, 2012; Wintrobe & Greer, 2004). In prokaryotes, hemes A, B, C, D, and O are common and considered 'true' hemes with their porphyrin rings containing a complete system of conjugated double bonds (Layer, 2021). Heme B is the precursor to all other types of heme found in biological systems and is the most versatile member of the heme family (Layer, 2020; Rich, 2012). Hemes A, C, D, and O are derivatives of heme B that vary by their porphyrin ring substituents (Layer, 2020; Rich, 2012). Other important heme members found in nature are hemes D1, I and M (Rich, 2012; Wintrobe & Greer, 2004). Heme B comprises the heme in heme proteins such as hemoglobin, myoglobin, and cytochrome P450 in humans (Rich, 2012). In addition to being the crucial component for oxygen transport and storage in hemoglobin and myoglobin, heme B from hemoglobin and myoglobin is the source of up to 50% of the total iron absorbed in the human body (Wintrobe & Greer, 2004). The initial precursor for the tetrapyrrole of heme B is 5-aminolevulinic acid, a small nonproteinogenic amino acid (Jiang et al., 2022; Layer, 2020; Wintrobe & Greer, 2004).

Depending on the heme type, the heme protein, and the required function, heme will be covalently or noncovalently bound (Schneider, Marles-Wright, Sharp, & Paoli, 2007). Further, the chemical and physical properties of heme can be tuned with the number of axial ligands coordinating the heme or with different types of amino acid residues neighboring the heme molecule in heme proteins (Layer, 2020; Schneider et al., 2007). The diversity of heme properties within heme proteins allows for vast biological functions across species and makes it a crucial molecule across life forms (Ferreira, 2013; Layer, 2020, 2021).

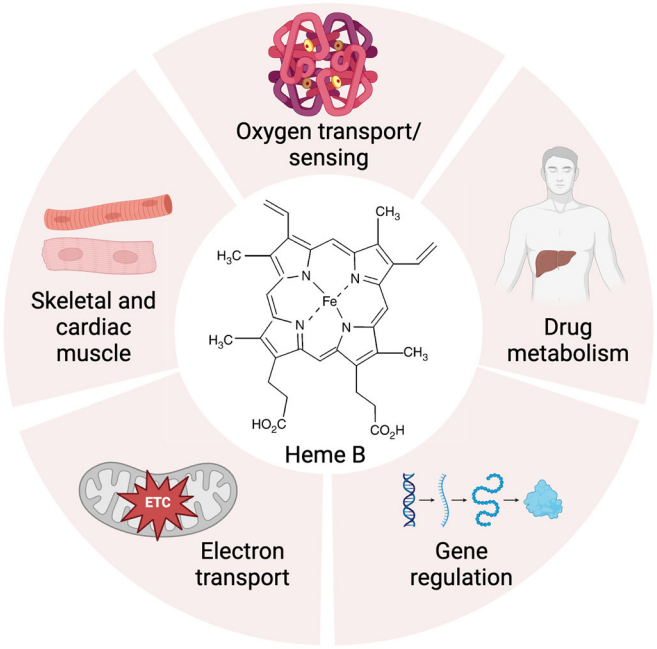

Figure 1. Structure of heme B with associated functions. Heme B, the precursor for all other biologically employed hemes, has a porphyrin ring with methyl groups at positions C1, C6, C11, and C17, propionic acids at C12 and C16, and vinyl groups at C2 and C7. Within the porphyrin macrocycle is an iron ion. Examples of biological functions of heme B include gas sensing and transporting, drug metabolism via complex chemical catalysis with P450 enzymes, signaling and transcription regulation, and electron transfer.

1.2 The Role of Aminolevulinic Acid Synthase in Heme Biosynthesis

For many biosynthetic pathways, the first enzymatic reaction producing the committed precursor to be incorporated into the anticipated biological compound is known as the committed step of biosynthesis (Ferrier, 2017). This generalization holds true for heme biosynthesis, in which the first step is irreversible (Hunter & Ferreira, 2011). The precursor for the tetrapyrrole ring of heme B is 5-aminolevulinic acid (ALA) (Hunter & Ferreira, 2011). The synthesis of ALA is the first and rate-limiting step of heme biosynthesis (Hunter & Ferreira, 2011). Depending on the species, ALA is synthesized by one of two pathways. In plants, most bacteria, and algae, ALA is synthesized by the C5 pathway, in which glutamate is the precursor for ALA. Glutamyl-tRNA is generated from glutamate for subsequent production of ALA (Cui, 2021; Jiang et al., 2022). In mammals, fungi and α-proteobacteria, ALA is synthesized through the C4 pathway (or the Shemin pathway) (Layer, Reichelt, Jahn, & Heinz, 2010). In the Shemin pathway, ALA is synthesized by the pyridoxal- 5'-phosphate (PLP)-dependent enzyme aminolevulinic acid synthase (ALAS) (Hunter & Ferreira, 2009; Layer et al., 2010). ALAS condenses glycine and succinyl-CoA into ALA (Cui, 2021). ALAS is the only enzyme involved in the production of ALA in the Shemin pathway (Hunter & Ferreira, 2009; Layer et al., 2010). In the C5 pathway, three enzymes are involved in the conversion of glutamate to ALA (Cui, 2021). ALAS in only found in α-proteobacteria in prokaryotes. Because α-proteobacteria are the group of bacteria from which mitochondria originated, it has been suggested that mitochondria formed from the transformation of an α-proteobacterium. Thus, mitochondria were equipped with eukaryotic ALAS when mitochondria organelles originated (Wintrobe & Greer, 2014).

ALAS is known as the gatekeeper for heme biosynthesis because all subsequent steps of the heme biosynthetic pathway depend on proper execution of this first step (Meguro, Igarashi, Yamamoto, Fujita, & Sassa, 1995; Sadlon, Dell'Oso, Surinya, & May, 1999; Stojanovski et al., 2019). For non-plant eukaryotes, ALAS produces ALA in the mitochondrial matrix, and the subsequent steps of heme biosynthesis continue in the cytosol. The last two steps of heme biosynthesis finalize in the mitochondrial matrix where ferrous iron is inserted into protoporphyrin IX (**Figure 2**) (Ferreira, 1995; Stojanovski, Hunter, Jahn, Jahn, & Ferreira, 2014). The reaction catalyzed by ALAS is highly exergonic, and tight regulation of heme biosynthesis occurs through ALAS. Additionally, expression of downstream heme biosynthetic enzymes is dependent on the expression of ALAS, further highlighting its critical role in heme production (Meguro et al., 1995).

1.3 ALAS Catalysis, Evolution, and Regulation

1.3.1 ALAS Catalytic Cycle

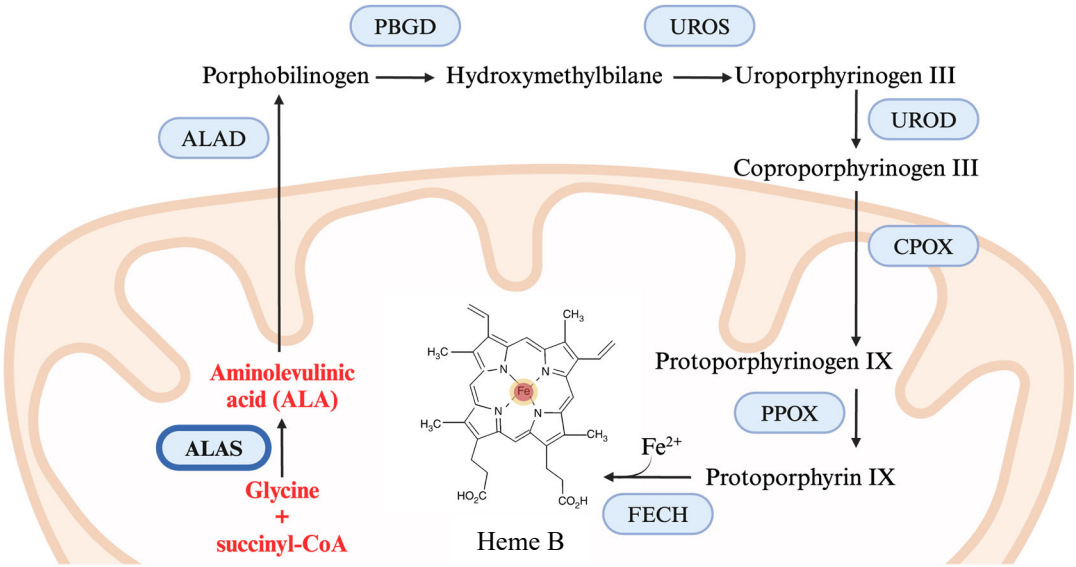

Figure 2. Eukaryotic heme biosynthesis pathway. Aminolevulinic acid synthase (*dark blue circle*) initiates heme biosynthesis in the mitochondrion of nonplant eukaryotes by catalyzing the condensation of glycine and succinyl-CoA to ALA (*red labels*). Other enzymes involved in the pathway are indicated in *light blue circles* whereas intermediates are labeled in *black*.

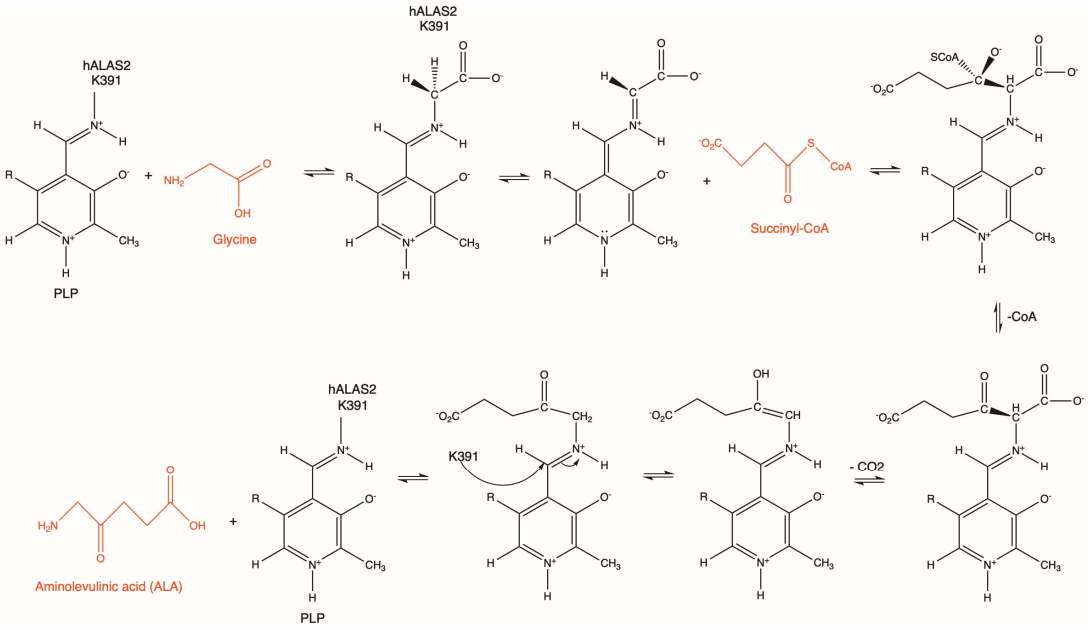

Figure 3. ALAS2 Catalytic Reaction. PLP covalently binds to the active site lysine 391 in the resting state. The reaction begins with the entry of glycine in the active site to forms an external aldimine. Loss of a proton from the α carbon of glycine forms the first quinonoid intermediate. Condensation with succinyl-CoA is accompanied with release of the CoA component. Decarboxylation of the α-amino-β-ketoadipic acid intermediate results in an enol intermediate. The enol intermediate interconverts to a second quinonoid intermediate of ALA. Finally, hydrolysis releases the ALA product.

ALAS is a PLP-dependent enzyme. It exists as a homodimer with PLP covalently linked to a conserved catalytic lysine residue as a Schiff base (Stojanovski et al., 2019). The reaction mechanism begins with entry of glycine and displacement of the Schiff base linkage (**Figure 3)**. Then, loss of a proton from the α carbon of glycine generates a carbanion intermediate. A Claisen condensation of the carbanion with succinyl-CoA leads to CoA release and an enzyme-bound intermediate (α-amino-β-ketoadipic acid). Finally, decarboxylation of this intermediate yields the quinonoid of ALA. Hydrolysis then liberates the release of ALA (**Figure 3**) (Stojanovski et al., 2014).

1.3.2 ALAS Evolution

ALAS has a conserved catalytic core that contains the active site where substrates bind and additional structural motifs that play a role in harmonious ALAS function (Brown, Kardon, Sauer, & Baker, 2018). Eukaryotes evolved N-terminal and C-terminal extensions that have high sequence diversity among organisms (Astner et al., 2005; Bailey et al., 2020; Brown et al., 2018). The N-terminal extension contains the mitochondrial targeting sequence, and the C-terminal extension is thought to play a regulatory role for ALAS. However, the function of the C-terminal extension is still being elucidated and may have differing roles in different species (Tran & Brown, 2023). Vertebrates have two isoforms of ALAS encoded by separate genes on separate chromosomes. These are ALAS1, the ubiquitously expressed isoform, and ALAS2, the erythroid specific isoform (Bishop, 1990; Bishop, Henderson, & Astrin, 1990; Cotter, Drabkin, Varkony, Smith, & Bishop, 1995). ALAS1 is encoded on chromosome 3, whereas ALAS2 is encoded on chromosome X, which leads to X-linked inheritance patterns of disease alleles (Cotter et al., 1995; Cox, Kozman, Raskind, May, & Mulley, 1992).

1.3.3 ALAS1 and ALAS2 Regulation

ALAS1 and ALAS2 differ primarily in their N and C-termini. The two isoforms are 66% similar and 60% identical. As seen in both isoforms, the catalytic domain is encoded by exons 5 to 11 (Taylor & Brown, 2022). One major difference in ALAS1 and ALAS2 is the presence of a 5' iron response element (IRE) in the mRNA of *ALAS2* (Ducamp et al., 2021; Wintrobe & Greer, 2004). This leads to a unique regulatory mechanism by iron for ALAS2 (Melefors et al., 1993). IREs are short hairpin structures that allow binding by iron regulatory proteins in accordance with cellular iron levels (Menotti, Henderson, & Kuhn, 1998). The ALAS2 gene promoter also contains a noncanonical TATA motif that binds GATA1, the master transcription factor for erythroid development, and TATA-binding protein for maximal expression (Meguro et al., 1995; Sadlon et al., 1999). The specificity of ALAS2 for erythroid cells coincides with a heavy heme requirement for erythropoiesis (Wintrobe & Greer, 2014). Thus, distinct regulatory mechanisms have evolved and are localized to the terminal ends of ALAS2 (Kaneko et al., 2014; Meguro et al., 1995; Sadlon et al., 1999).

A.

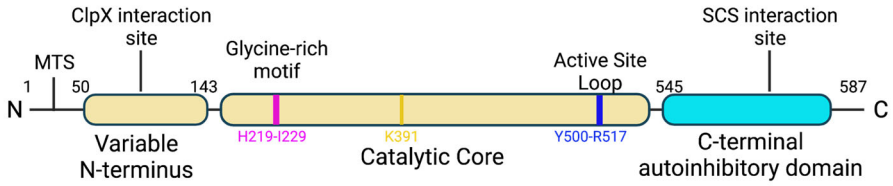

B.

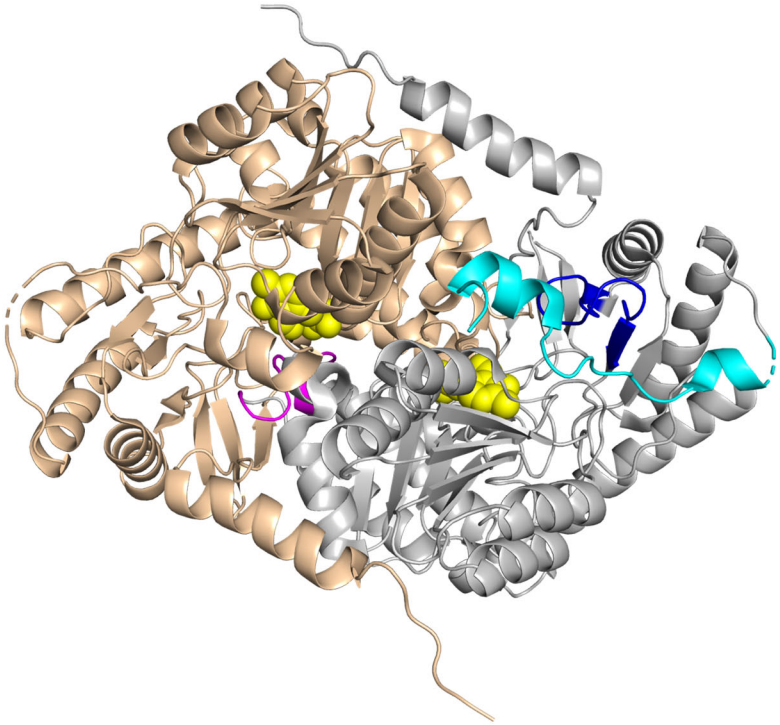

Figure 4. Domain map and structure of human ALAS2 homodimer with important structural elements denoted in pink, teal, and blue. A. Domain map with amino acid residues noting major structural regions. N-terminal domain is made up of amino acid residues 1-142. The conserved catalytic core containing the glycine-rich motif (pink), catalytic lysine (yellow), and active site loop (blue) is made up of amino acid residues 143-544. Finally, the C-terminal domain is made up of amino acid residues 545-587. B. Each monomer of ALAS2 is represented as wheat and gray. PLP cofactor represented in yellow as spheres. Glycine-rich loop is represented in pink and the active site loop is represented in blue. The eukaryotic-specific, autoinhibitory C-terminal extension is shown in teal (Taylor & Brown, 2022). PDB: 6HRH.

1.4 ALAS2 Structure and Disease

1.4.1 ALAS2 Structural Elements

Human ALAS2 is a homodimer with each protomer containing an N-terminal region (amino acids 1– 142) that harbors the mitochondrial targeting sequence, a catalytic core (amino acids 143–544) containing the PLP cofactor and active site, and a C-terminal extension (amino acids 545–587) (**Figure 4)** (Bailey et al., 2020; Taylor & Brown, 2022). The glycine-rich motif (amino acids His219-Ile229) helps to mediate cofactor and substrate binding (Gong & Ferreira, 1995). This region is flexible in the absence of PLP cofactor and becomes ordered upon PLP incorporation (Brown et al., 2018). Arg227 mediates a salt bridge with Glu240 that restricts the dynamics of this loop and caps the substrate-binding pocket (Bailey et al., 2020). Lys391 at the active site forms a covalent Schiff base with the PLP cofactor to activate the enzyme for catalysis (Ferreira, Neame, & Dailey, 1993). The active site loop is comprised of residues Tyr500-Arg517. This region provides the regulatory gate for ALA product release (Lendrihas, Hunter, & Ferreira, 2010). The active site loop interacts with the eukaryote-specific C-terminal extension (**Figure 5**). The C-terminal extension impacts ALA release during catalysis and restricts movement of the active site loop through a salt bridge network (Bailey et al., 2020; Hunter & Ferreira, 2022). The salt bridge network is between residues Asp159 of the catalytic core, Arg511 of the active site loop, and Glu569 of the C-terminal extension (**Figure 5**). This salt bridge network must be disrupted to access the catalytic residues for both substrate binding and product release, imposing an autoinhibitory function of the C-terminal extension in ALAS2 (Bailey et al., 2020; Hunter & Ferreira, 2022).

1.4.2 ALAS2 and Disease

ALAS2 is responsible for synthesizing up to 90% of the total body's heme for hemoglobin (Stojanovski et al., 2019). The role of ALAS2 in the production of hemoglobin makes it a critical and sensitive enzyme for healthy red blood cell development. More than 90 disease-associated mutations in ALAS2 have been reported (Taylor & Brown, 2022). Over 85% of the disease mutations are reported as missense mutations (Taylor & Brown, 2022). The other mutations manifest as insertions or deletions in the promoter region of the *ALAS2* gene, lead to alternative splice variants, or cause frameshifts (Balwani, 2019; Ducamp et al., 2021; Tchaikovskii, Desnick, & Bishop, 2019; Whatley et al., 2008). Two blood disorders in humans manifest from ALAS2 mutations (Dailey & Meissner, 2013). The first disorder is X-linked protoporphyria (XLPP), in which gain-of-function mutations stem from truncations or frameshifts that alter the eukaryote-specific C-terminal extension (Sassa, Akagi, Nishitani, Harigae, & Furuyama, 2002). In XLPP, a pernicious buildup of heme intermediates causes photosensitivity and severe pain in the skin (Balwani, 2019). The second disorder is X-linked sideroblastic anemia (XLSA), in which loss-of-function mutations in ALAS2 lead to heme biosynthesis dysfunction (Ducamp & Fleming, 2019). During the development of XLSA, heme biosynthesis is impaired, but iron continues to be transported to the mitochondria

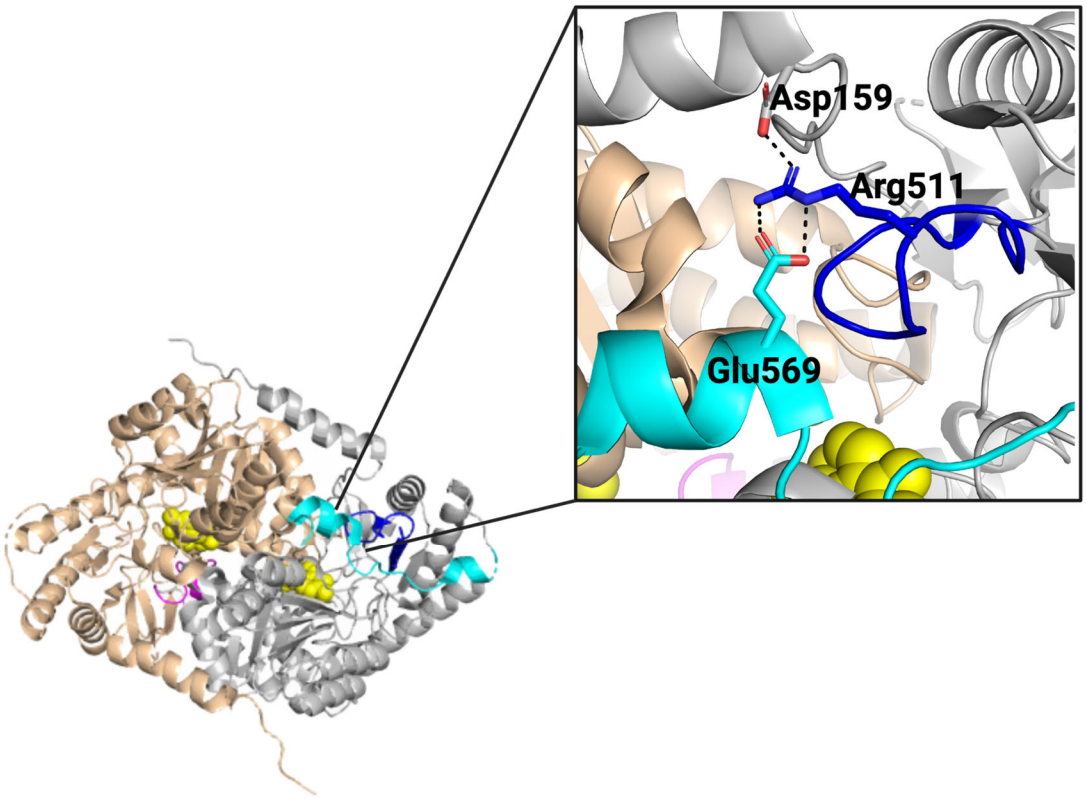

Figure 5. Structure of human ALAS2 homodimer with the salt bridge between the C-terminal extension and the active site loop highlighted in the inset. Each monomer of ALAS2 is represented in wheat and gray as in Figure X. PLP cofactor is represented as yellow spheres. The glycine-rich loop is represented in pink, and the active site loop is represented in blue. The eukaryotic-specific, autoinhibitory C-terminal extension is shown in teal. The salt bridge between the C-terminal extension and the active site loop consists of amino acid residue Glu569 of the C-terminal extension, Arg511 of the active site loop, and Asp159 of ALAS2 monomer. PDB: 6HRH.

(Bottomley, May, Cox, Cotter, & Bishop, 1995; Mollin, 1965). This leads to a toxic buildup of iron in the mitochondria and, in the most severe cases, in the pancreas, heart, and liver (Tian, Zhao, Xiong, Yu, & Du, 2023). The accumulation of iron can cause irreversible organ damage and lead to fatal outcomes (Finlayson, 1990; Scimeca, Weinblatt, & Kahn, 1994). Successful treatments for XLSA include phlebotomy, chelation, pyridoxine supplementation, and recently, gene editing (Fang et al., 2021; May & Bishop, 1998; May & Fitzsimons, 1994). Pyridoxine is metabolized to the active form of PLP in the liver (Merrill & Henderson, 1990). While phlebotomy and chelation target iron overload associated with heme biosynthesis dysfunction, pyridoxine supplementation is the primary treatment for XLSA that ALAS2 function. However, other factors such as metabolism, age, and diet contribute to an individual's responsiveness to pyridoxine (Barton & Lee, 2006; Cazzola et al., 2002; Prades et al., 1995).

1.5 Scope of Dissertation

This dissertation consists of two projects. In Chapter II, I present a mutational analysis of ALAS2 disease alleles to elucidate the molecular details underlying loss-of-function in patients suffering from XLSA. I specifically focus on mutations in the C-terminal extension of ALAS2. The C-terminal extension is not well conserved across organisms, and truncation of the C-terminal extension has opposite effects in yeast ALAS than in human ALAS2, further exemplifying its interesting characteristics. Additionally, truncations or frameshift mutations of the C-terminal extension lead to hyperactivity in all clinical cases. However, a small number of loss-of-function mutations in the C-terminal mutations are reported. It was my goal to identify the molecular details of how the C-terminal extension is implicated in a loss-of-function disease.

In Chapter III, I describe my investigation of a previously reported binding partner for ALAS2. The proposed interaction was shown previously to be disrupted by specific XLSA mutations. My goal was to probe the interaction between WT ALAS2 and the binding partner and characterize the binding with various binding assays. I measured the binding affinity using microscale thermophoresis which suggested a loose interaction. Subsequent experiments corroborated the conclusion that the two proteins interact weakly. Another conclusion was that perhaps there is an additional factor that is needed for a strong interaction to be captured. Together, this research provides molecular details about ALAS2 and the underlying mechanisms leading to XLSA that were previously unknown. In addition to isolating the molecular details underlying enzyme dysfunction, I revealed specific information on how human ALAS2 may differ from other organisms through loss of function mechanisms originating in the C-terminal extension. These data contribute to our understanding of ALAS2 clinically and evolutionarily. Additionally, the analysis of ALAS2 and its putative binding partner reveal the critical next steps that must be taken to continue investigating the interaction. Thus, these results reveal key information about heme biosynthesis and regulation.

CHAPTER 2

C-terminal XLSA ALAS2 Mutations and Their Role in Enzyme Dysfunction[1]

2.1 Introduction

Heme is a critical biomolecule involved in necessitous processes such as drug metabolism, oxygen transport, and electron transport (Chiabrando et al., 2014). Harmonious heme production is critical for healthy red blood cell production. The criticality of proper heme production is highlighted in blood diseases where heme biosynthesis is disrupted (Cotter, Rucknagel, & Bishop, 1994; Dailey & Meissner, 2013; Sassa et al., 2002; Thomas, Visanica, Poussing, Gerard, & Perrin, 2023). The first and rate-limiting step of heme biosynthesis is catalyzed in the mitochondria by aminolevulinic acid synthase (ALAS) (Ferreira & Gong, 1995). ALAS condenses glycine and succinyl-CoA into aminolevulinic acid (ALA) (Stojanovski et al., 2019). ALAS is known as the gatekeeper for heme biosynthesis because all subsequent steps of the heme biosynthetic pathway depend on proper execution of this first step (Hunter & Ferreira, 2011). In addition, the expression of downstream heme biosynthetic enzymes is dependent on the expression of ALAS, further highlighting its critical role in heme production (Meguro et al., 1995).

ALAS is conserved among α-proteobacteria and non-plant eukaryotes. Vertebrates have two isoforms of ALAS that are encoded by separate genes on separate chromosomes (Bishop, 1990). These are ALAS1, the ubiquitously expressed isoform, and ALAS2, the erythroid specific isoform (Bishop, 1990; Bishop et al., 1990; Cotter et al., 1995). ALAS2 is localized to developing red blood cells and takes on the heavy heme requirement for erythropoiesis (Ferreira & Gong, 1995). The increased heme burden that ALAS2 assumes in erythropoiesis coincides with different regulatory mechanisms from ALAS1 (Cox, Bawden, Martin, & May, 1991; Peoc'h et al., 2019). For example, ALAS2 expression is regulated by cellular iron levels through iron-response elements, which is unique to ALAS2 as compared to ALAS1 and other heme biosynthetic enzymes (Cox et al., 1991; Peoc'h et al., 2019). Tragically, ALAS2 is linked to blood diseases that afflict men and women of all ages that can be fatal (Nzelu et al., 2021; C. Rose et al., 2017).

The role of ALAS2 in the synthesis of total heme for hemoglobin makes it a critical enzyme for the production of healthy red blood cells (Stojanovski et al., 2019). This is highlighted by the >90 reported mutations in

[1]This chapter contains previously published data from "Elucidating the role of human ALAS2 C-terminal mutations resulting in loss-of-function and disease" published in Biochemistry and has been reproduced with the permission of the publisher and my co-author Breann Brown, Ph.D. | Citation: Taylor, J. L., Ayres-Galhardo, P. H., & Brown, B. L. (2024). Elucidating the Role of Human ALAS2 C-terminal Mutations Resulting in Loss of Function and Disease. *Biochemistry*. doi:10.1021/acs.biochem.4c00066

ALAS2 that lead to heme biosynthesis dysfunction and blood disease (Taylor & Brown, 2022). Two blood disorders manifest from ALAS2 mutations (Balwani, 2019; Balwani & Desnick, 1993; Pereira, Barbot, & Ribeiro, 2009). The first is X-linked protoporphyria, in which gain-of-function mutations localize to the C-terminal extension of the enzyme. The second is X-linked sideroblastic anemia (XLSA), in which loss-of-function mutations arise throughout the *ALAS2* gene (Balwani, 2019; Balwani & Desnick, 1993; Pereira et al., 2009). During the development of XLSA, heme biosynthesis is impaired, but iron continues to be transported to the mitochondria (Bottomley et al., 1995; Mollin, 1965). This leads to a toxic buildup of iron in the mitochondria and eventually, in the most severe cases, in the pancreas, heart, and liver (Tian et al., 2023; Wintrobe & Greer, 2004). The accumulation of iron can cause irreversible organ damage and lead to fatal outcomes (Ashorobi & Chhabra, 2024). Over 90 ALAS2 mutations lead to XLSA, but the molecular basis for disease is unknown for the majority of the mutations. Dissecting the molecular basis for XLSA allows us to understand what enzymatic defects underlie the disease. This information will not only provide the molecular information for enzyme dysfunction, but it magnifies the specific enzymatic defect in XLSA that can be pharmacologically targeted in the future for XLSA treatment. Pyridoxine, the main treatment option for XLSA, is not effective in many XLSA cases (Donker et al., 2014; Furuyama et al., 2006; Taylor & Brown, 2022).

The terminal 42 amino acids make up the C-terminal extension in human ALAS2 (Bailey et al., 2020). The formation of a critical salt-bridge between the C-terminal extension and the active-site loop of ALAS2 awards it an auto-inhibitory role on enzyme activity because the salt bridge must be disrupted for complete catalysis to occur (Bailey et al., 2020; Ducamp et al., 2013). The C-terminal extension is not conserved across organisms. Truncation of the C-terminal extension has opposite effects in yeast ALAS than in human ALAS2, further exemplifying its interesting characteristics (Brown et al., 2018; Tran & Brown, 2023). All gain-of-function ALAS2 mutations in humans are localized to the C-terminal extension. Yet, a small percentage of XLSA loss-of-function mutations have been identified in this region (Taylor & Brown, 2022). Beyond mutations disrupting the salt-bridge, how any one mutation in the C-terminal extension leads to either gain-of-function or loss-of-function is not clear. Here, I dissect C-terminal mutations V562A and M567I in ALAS2. The two C-terminal XLSA loss-of-function mutations were identified in a concurrent study of ALAS2 (Kadirvel et al., 2012). These mutations were identified in independent male probands aged 14 and 36 that exhibited iron overload and reduced hemoglobin levels (Kadirvel et al., 2012). In addition to causing a loss-of-function phenotype in a seemingly autoinhibitory region of the enzyme, these mutations are uncharged, hydrophobic mutations in the C-terminal extension. This eliminates the ability to form polar contacts in the region that could interfere with the flexibility or function of the C-terminal extension.

These mutations were previously shown to impair enzyme activity in mitochondria of transfected HEK293

cells (Kadirvel et al., 2012). Further, the mutations exhibited varying *in vitro* enzymatic activity, but as is the case with most XLSA mutations, the molecular details of enzyme dysfunction have not been elucidated. I aimed to uncover the molecular details of V562A and M567I mutants that cause impaired heme biosynthesis. This investigation informs our mechanistic understanding of how C-terminal ALAS2 mutations impair enzyme function, as opposed to enhancing it as seen in many C-terminal defects of ALAS2. From this study, I isolated the molecular defects of each mutant enzyme and used this information to broaden our understanding of ALAS2 C-terminal extension mutations in XLSA. Further, I identified two separate modes of enzyme dysfunction from XLSA mutations that clarified how heme biosynthesis is differentially disrupted in the disease.

2.2 Results

2.2.1 Hydrophobic C-terminal Mutations Significantly Impact Protein Stability

2.2.1.1 Structural Analysis

The V562A and M567I ALAS2 mutations were initially identified in male subjects that were 14 and 36 years of age, respectively. The patients exhibited microcytic hypochromic anemia with iron overload and reduced hemoglobin levels. For most XLSA mutations, the molecular basis of ALAS2 dysfunction underlying disease is poorly understood. The obscurity is confounded by varying degrees of disease severity, widespread 3-dimensional location of the mutations, or variable patient responsiveness to treatment (Barton & Lee, 2006; Taylor & Brown, 2022). I examined the V562A and M567I ALAS2 variants to determine how the mutations impact enzyme structure, stability, cofactor binding, and enzyme kinetics to further understand how ALAS2 mutations lead to XLSA.

I first used computational tools to visualize these residues in the ALAS2 structure (**Figure 6**). As seen in Figure 4, amino acids Val562 and Met567 reside on the middle and terminal regions of the C-terminal extension. Val562 is in a widely solvent accessible region of the structure. According to the crystal structure, the nearest residues to Val562 are at least four angstroms away. One potential structural implication of replacing a valine with an alanine is that this could create a more flexible span of residues as a result of reducing the size of the amino acid side chain (**Figure 6A**). The region could rotate with less steric hindrance if the amino acid side chain is smaller. However, this is only a speculation, and there are no glaring structural implications of mutating Val562 to Ala562. Mutating Met567 to an Ile567 removes the sulfur on the aliphatic chain of the amino acid side chain. I hypothesize that this alteration would reduce the electronegativity of this region by removing the sulfur from the side chain (**Figure 6B**). Met567 is alongside the α-helix harboring Glu569 that is used in the autoinhibitory salt bridge, but it does not make any direct contact with the salt

A. **Val562 Visualized on ALAS2 Structure for Structural Insight**

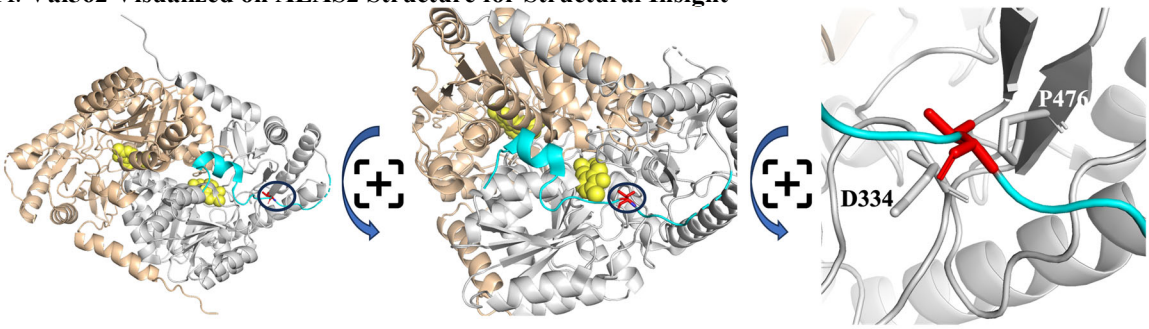

B. **Met567 Visualized on ALAS2 Structure for Structural Insight**

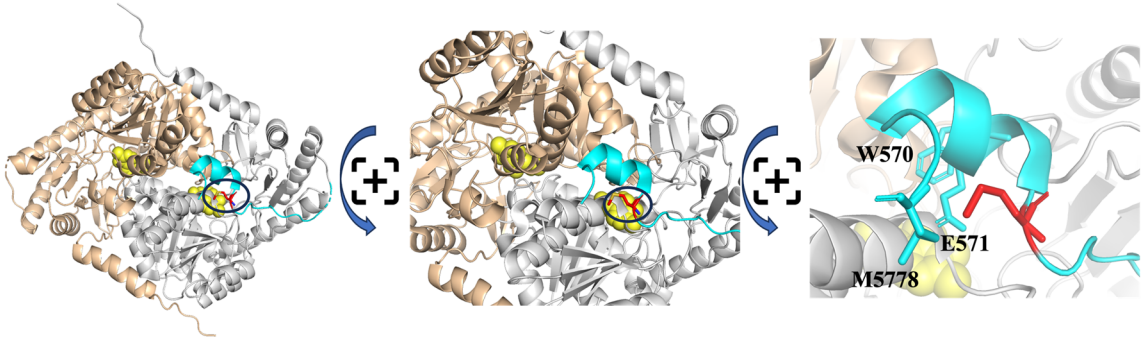

Figure 6. Affected XLSA residues visualized on ALAS2 structure at different angles. ALAS2 monomers represented in wheat or gray; PLP cofactor displayed as yellow spheres; C-terminal extension represented on one monomer in cyan; residue of interest is marked and represented as sticks in red with nearest residues represented as sticks. Each panel from left to right is zoomed in for ease of visualization. A. Val562 is highlighted on ALAS2 structure. B. Met567 is highlighted on ALAS2 structure.

bridge residue. Mutating Met567 to Ile567 may alter the microenvironment of this residue, but there are no obvious structural consequences. Based on structural insights, the 3-dimensional location of each mutation is insufficient for understanding enzyme dysfunction.

I isolated the mature form of the mutant proteins (amino acids 54-587) from BL21-DE3-RIL cells that excludes the mitochondrial targeting sequence. I first determined if there were any major secondary structure deviations in the mutants compared to WT ALAS2. Analysis of the far-UV CD spectrum of each variant revealed a well-conserved secondary structure in the mutants compared to WT (**Figure 7**), indicating that there are no major secondary structure changes with V562A and M567I mutations in ALAS2.

2.2.1.2 Stability Analysis

I next asked whether the mutations would destabilize the mutant proteins leading to impaired enzyme function. According to the DeepDDG server which predicts the stability change of point mutations on proteins, both V562A and M567I mutations would be mildly destabilizing with DDG values of -1.589 and -0.772, respectively (Cao, Wang, He, Qi, & Zhang, 2019). This prediction anticipates V562A to be slightly more destabilizing than M567I. To measure the stability of the mutant proteins, I employed differential scanning fluorimetry and determined unfolding temperatures (T_m) of the mutants compared to WT. I found that the WT and M567I holoenzymes had similar T_m values (~49.7°C) with V562A having a T_m approximately 3°C lower than the other constructs (**Figure 8A**). This suggests that the introduction of V562A destabilizes ALAS2 *in vitro*, whereas the introduction of M567I does not affect *in vitro* protein stability. The ALAS2 cofactor, pyridoxal phosphate (PLP), is required for catalysis, and PLP supplementation is a standard treatment for XLSA patients. For some XLSA variants, the addition of PLP increases enzymatic activity and has also been suggested to have stabilizing effects on the enzyme. I therefore tested whether V562A and M567I mutant proteins are stabilized by adding exogenous PLP (**Figure 8B)**. The addition of excess PLP resulted in a significant increase in protein stability of ~6°C for all variants. To further probe the impact of PLP on the mutants, I generated the apoenzymes of the variants. I found that WT and M567I apoenzymes had decreased T_m values compared to their holo counterparts (**Figure 8D**). The apo M567I variant exhibited the largest decrease in T_m compared to the holoenzyme and the largest response to the addition of PLP, with a 16°C increase in T_m. Exogenous PLP stabilized the WT apoenzyme by approximately 9°C, and the V562A variant showed the lowest PLP-induced stability resulting in a 7°C increase in T_m.

2.2.2 PLP Binding is Altered in V562A and M567I

2.2.2.1 PLP Tautomeric States

Given that PLP binding is critical for catalysis and the stability of V562A and M567I was impacted by PLP

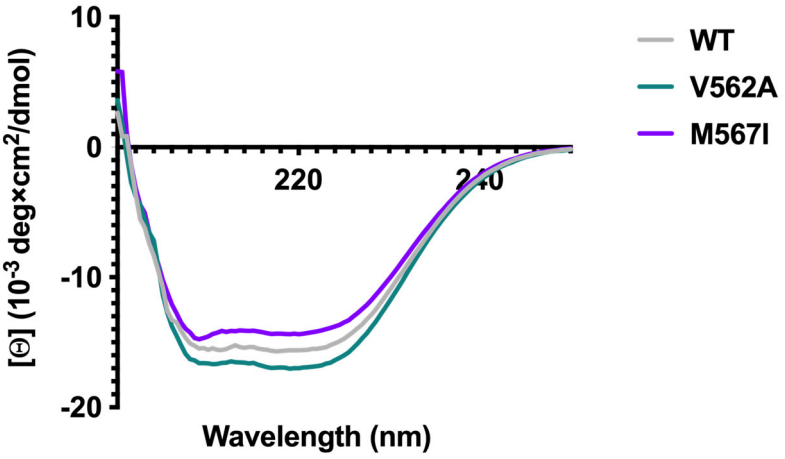

Figure 7. Secondary structure analysis by circular dichroism reveal no major changes in secondary structure for the disease variants. Circular dichroism polarimetry analysis of WT (gray), V562A (teal), and M567I (purple) ALAS2 variants.

A. **T_m Analysis of Holo Variants** B. **T_m Analysis of Holo Variants with PLP**

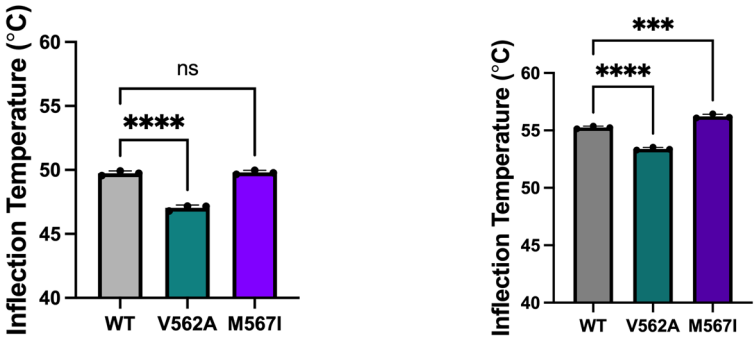

C. **Combined T_m Analysis of Holo Variants ± PLP**

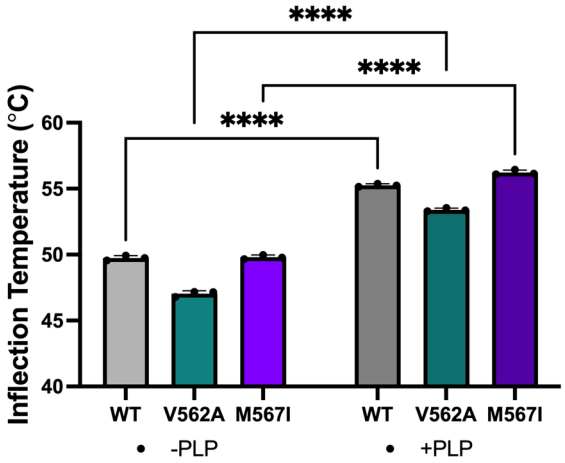

D. **Combined T_m Analysis of Apo Variants ± PLP**

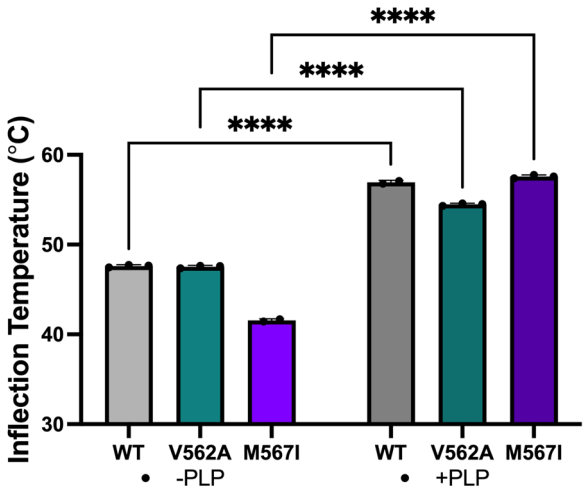

Figure 8. Unfolding temperatures of holo and apo variants indicate C-terminal mutations significantly impact protein stability. A) Unfolding temperatures of holo variants assayed by differential scanning fluorimetry in the absence or B) presence of exogenous PLP. C) Comparison of unfolding temperatures with or without PLP for holo or D) apo variants. (***p<0.0008, ****p<0.0001)

to varying degrees, I aimed to characterize the nature of the bound cofactor in the variants. As such, I monitored the PLP profiles of each mutant compared to WT. PLP binds a catalytic lysine, Lys391, in human ALAS2. For ALAS2 and other fold type-2 PLP-binding proteins, PLP binds as a mixture of species (**Figure 9A**) (Fasella, 1967). PLP binds as ketoenamine, substituted aldimine, and enolimine tautomers (**Figure 9A**). The significance of the various tautomeric forms is that the ketoenamine and enolimine forms are in the proper hybridization state to accept a proton from glycine which initiates the first step of enzymatic catalysis (Stojanovski et al., 2014). These are the "active" forms of PLP. The substituted aldimine is considered the "inactive" form, as it must undergo electron rearrangement for catalysis. The various PLP tautomers are observed with spectroscopy (**Figure 9B**). Using UV-Vis spectroscopy, I monitored the PLP binding states of V562A and M567I compared to WT ALAS2. We found the presence of both 326 nm and 424 nm peaks for V562A and M567I, which correspond to both the inactive and active forms of PLP (**Figure 9B**). The mutants follow a similar spectral profile as WT (**Figure 9B**).

As a proxy for total PLP bound per protein unit, I summed the total absorbance units from 326 nm and 424 nm and normalized the absorbance values with the concentration of each protein construct, respectively. Using this metric, I observed that M567I has significantly less PLP bound per protein unit compared to V562A, which has the same total PLP bound per protein unit as WT (**Figure 9C**).

Following the results of the UV-Vis experiments, I parsed out the PLP species that correspond to the 326 nm and 424 nm UV-Vis peaks with fluorescence spectroscopy (**Figure 10**). The substituted aldimine and the enolimine absorb at 326 nm. By exciting at 326 nm, each species can be observed at emission wavelengths of 370 nm for the substituted aldimine or 510 nm for the enolimine. Using this intrinsic property of the tautomers, I found that the species comprising 326 nm peak for V562A and M567I is the substituted aldimine or the "inactive" species (**Figure 10A**). For V562A and M567I, the species comprising 424 nm peak is the ketoenamine or the "active" species (**Figure 10C**). These results align with WT, which has the same PLP composition (**Figure 10A,C**). Quantifying the fluorescence spectra revealed that for both mutants the substituted aldimine is present in significantly lower amounts than WT (**Figure 10B**). However, for V562A, the ketoenamine species is present in significantly higher amounts compared to WT (**Figure 10D**). This is in contrast to M567I which exhibits a significantly lower amount of the ketoenamine species. By representing the fluorescence data in percentages, I found that the ketoenamine species for V562A is 68% of the total relative fluorescence units (RFU). The ketoenamine species for M567I is 54% of the total RFU. Taken together, these data show that although the PLP spectral profiles for the mutants are similar to WT, the nature of PLP bound for the disease variants is significantly different from WT.

2.2.2.2 PLP Affinity

The PLP cofactor forms and stabilizes catalytic intermediates (**Figure 2**). It also is inserted during enzyme

A. **Tautomeric States of PLP with Corresponding Absorbance Wavelengths**

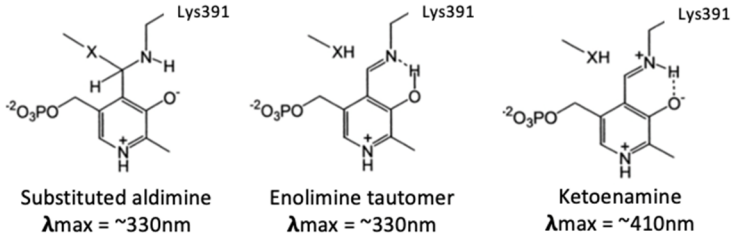

B. **Absorbance Spectra for Variants**

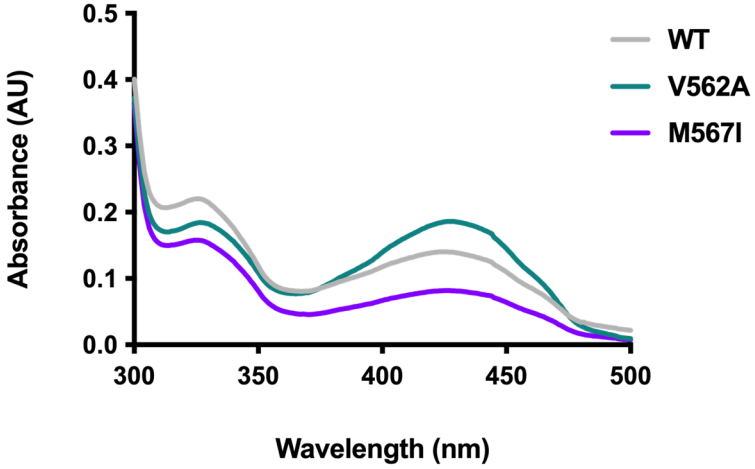

C. **Quantification of Total PLP for Variants**

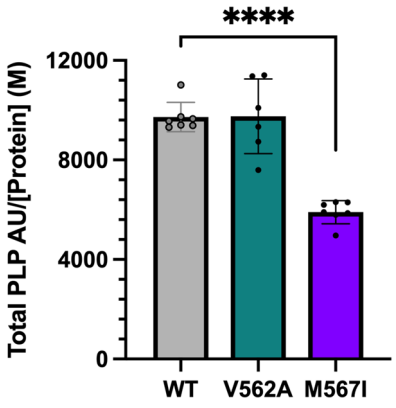

Figure 9. Absorbance scans of mutants follow characteristic PLP spectra. A) Tautomeric forms of PLP with their corresponding absorbance wavelengths. B) UV-Visible absorption spectra of hALAS2 WT (gray), V562A (teal), and M567I (purple) from 300-500 nm. C) Quantification of total PLP absorbance units for each construct normalized to protein concentration. (****p<0.0001)

A. **Fluorescence Emission Probing the 326 nm Species** B. **Quantification of (A)**

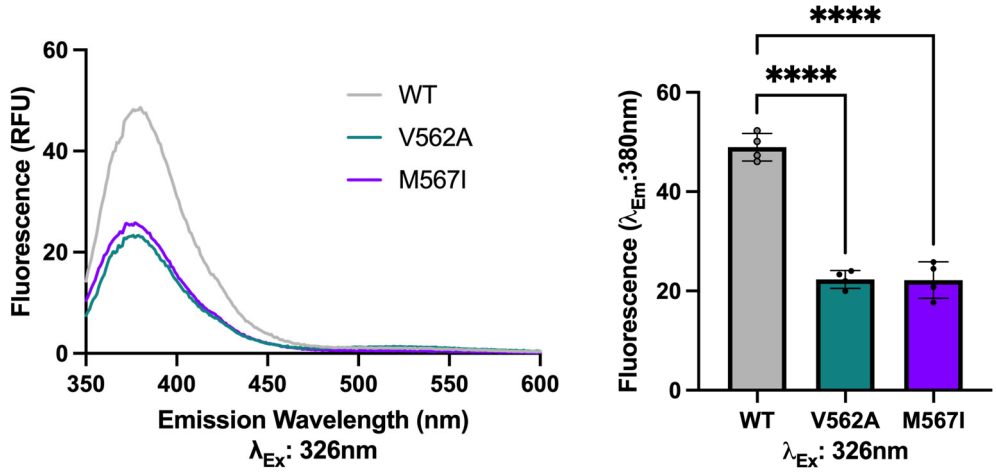

C. **Fluorescence Emission Probing the 424 nm Species** D. **Quantification of (C)**

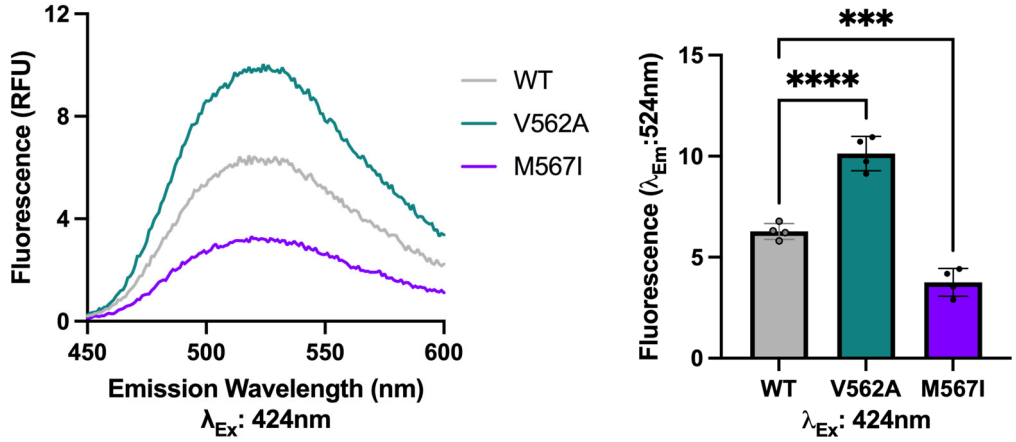

Figure 10. Fluorescence spectra of variants parse out PLP tautomeric species of 326 nm and 424 nm absorbance peaks. A) Fluorescence emission spectra from 350 nm-600 nm for WT (gray), V562A (teal), and M567I (purple) at 30 μM reveal the presence of one PLP tautomer at 326 nm corresponding to the substituted aldimine species. B) Quantification of fluorescence emission spectra from the 326 nm excitation wavelength indicate that V562A and M567I mutant have lower fluorescence values than WT. C) Fluorescence emission spectra from 450 nm-600 nm for WT (gray), V562A (teal), and M567I (purple) at 30 μM reveal the presence of the ketoenamine form of PLP for all constructs. D) Quantification of fluorescence emission spectra from the 424 nm excitation wavelength indicate that V562A has a higher amount of bound PLP in the ketoenamine state than WT or M567I (****$p<0.0001$).

folding. So far, the data show that PLP occupancy is altered in the disease variants (**Figures 9,10**). I next asked whether the affinity for PLP in the mutant proteins is changed. Using the apoenzymes and measuring ALA production as a function of PLP concentration, I found that WT hALAS2 binds PLP with a high nanomolar binding constant of approximately 400 nM (**Figure 11, Table 1**). Although both variants displayed nanomolar PLP binding affinity, the values were elevated compared to WT. Despite the higher K_M, the M567I variant had a faster catalytic rate (k_{cat}), which resulted in a comparable catalytic efficiency as WT. Interestingly, the V562A variant had the largest defect in affinity but ~6 times higher maximum enzyme velocity and faster k_{cat} compared to WT. This variant was also an order of magnitude more efficient than WT (**Table 1**).

Table 1. PLP kinetic parameters of ALAS2 variants

	WT	**V562A**	**M567I**
PLP			
V_{max} (U/mg)*	2469 ± 157	15562 ± 851	3781 ± 31
K_M (nM)	413 ± 63	653 ± 74	542 ± 17
k_{cat} (sec^{-1})	$3.4x10^{-4} \pm 2x10^{-5}$	$2.1x10^{-3} \pm 1x10^{-4}$	$5.17x10^{-4} \pm 4x10^{-6}$
k_{cat}/K_M ($sec^{-1}M^{-1}$)	823	3216	1055

*U measured as nmol of ALA produced per hour

2.2.3 ALAS2 Variants Have Disparate Steady-State Properties

2.2.3.1 Maximum Enzyme Activity is Unchanged by PLP

Given that the mutations are in the autoinhibitory C-terminal extension, I asked if they would impact enzymatic activity. Using a colorimetric endpoint assay, I measured the amount of ALA produced by each variant and WT (**Figure 12, Table 2**). By implementing saturating substrate concentrations, I aimed to overcome any rate impediments that may arise from working with loss-of-function mutations. I found that V562A has enhanced activity compared to WT with a V_{max} of 22,496 ± 4005 nmol/h/mg, demonstrating a 93% increase in V_{max} compared to WT (**Table 2**). In contrast, M567I displayed a diminished V_{max} of 8170 ± 991 nmol/h/mg demonstrating a 30% decrease compared to WT. The diminished enzymatic activity observed for M567I aligns with heme biosynthesis dysfunction when considered in a biological context. V562A has more of its total PLP occupied in the "active" state, as seen in the fluorescence spectra. Perhaps the higher percentage of PLP in the "active" state indicates a preference for PLP to exist in the active state for V562A.

Table 2. Specific activity of ALAS2 variants with saturating PLP

	No PLP	Percent change*	Plus PLP (10 μM)	Percent change
WT	11662 ± 1591	--	11754 ± 596	--
V562A	22496 ± 4005	+93%	24689 ± 3254	+110%
M567I	8170 ± 991	-30%	9663 ± 795	-18%

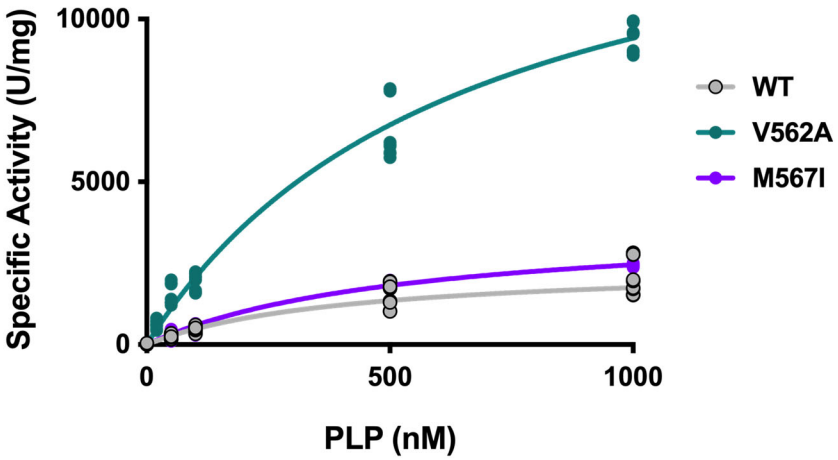

Figure 11. PLP binding kinetics for hALAS2 variants. PLP binding curves for apoenzymes of WT and mutants were determined with enzyme activity as a function of PLP concentration. Plot of specific activity (y-axis) with PLP concentration (x-axis). Binding curves for WT (gray), V562A (teal), and M567I (purple) are displayed. Data was fit using Michaelis-Menten model in Prism. PLP K_m for wild type is 413 nM ± 63 nM. PLP K_m for V562A is 653 nM ± 74 nM. PLP K_m for M567I is 542 nM ± 17 nM.

A.

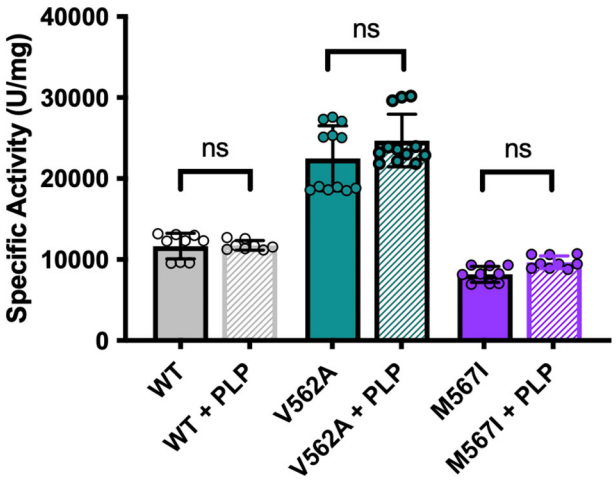

B.

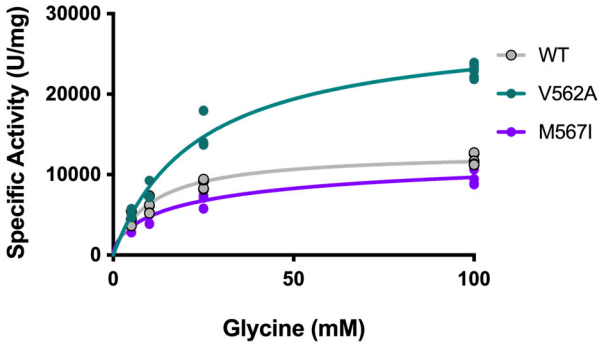

C.

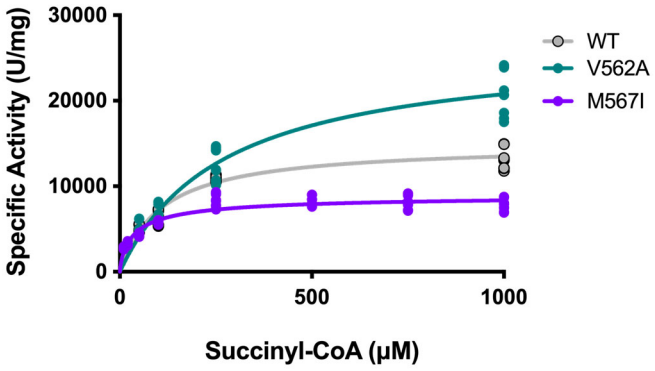

Figure 12. Steady-state activity and substrate kinetics of ALAS2 variants. A) Maximum enzyme activity for WT (grey), V562A (teal), and M567I (purple) was determined under saturating substrate concentrations in the absence (solid bars) or presence (hatched bars) of PLP. The addition of excess PLP did not affect activity for WT or the mutants. (ns=not significant). B) Plot of specific activity (y-axis) with glycine concentrations (x-axis). Kinetic curves for wild type (gray), V562A (teal), and M567I (purple) are displayed. Data was fit using Michaelis-Menten model (WT and V562A) or Allosteric Sigmoidal (M567I) model in Prism. C) Plot of specific activity (y-axis) with succinyl-CoA concentrations (x-axis). Kinetic curves for wild type (gray), V562A (teal), and M567I (purple) are displayed. Data was fit using Michaelis-Menten model (WT and V562A) or Allosteric Sigmoidal (M567I) model in Prism.

This may afford an explanation for enhanced enzymatic activity for V562A in saturating substrate conditions. Interestingly, a similar trend was observed in a yeast ALAS construct (Hem1) where PLP occupied more of the "active" state and enhanced activity was observed (Tran & Brown, 2023). A more active enzyme for V562A does not explain impaired heme biosynthesis, but it exemplifies that XLSA mutations impact enzyme function in various ways.

2.2.3.2 Binding Affinity of Substrates Reveals Insight into Enzyme Dysfunction

Beyond PLP binding, enzymatic defects can extend to substrate binding. Given that the V_{max} was determined with saturating substrate concentrations, I assessed enzyme kinetics under steady-state conditions with varying glycine or succinyl-CoA concentrations (**Figure 12 B-C, Table 3**). For glycine binding, hALAS2 V562A had a ~2-fold higher K_M compared to WT. Despite the higher K_M, the faster k_{cat} resulted in a catalytic efficiency similar to WT. For succinyl-CoA, the V562A variant had impaired succinyl-CoA binding. The K_M was 2.5 times higher than WT. The higher activity (V_{max}) for V562A was at the expense of significantly diminished binding affinity for succinyl-CoA and slightly diminished binding affinity for glycine (**Table 3**).

The M567I variant exhibited different kinetic characteristics compared to WT and V562A (**Table 3**). Although the M567I K_M (glycine) was elevated like V562A, the V_{max} was closer to WT and the k_{cat} was significantly diminished. Combined, this led to very inefficient catalysis concerning glycine. The M567I variant bound succinyl-CoA more readily, with a ~2.6-fold lower K_M than WT, although the catalytic efficiency remained unaffected. Importantly, M567I displayed negative cooperativity in binding both glycine and succinyl-CoA with Hill coefficients of 0.7± 0.1 and 0.78 ± 0.07, respectively. This would indicate that the binding of substrate at one of the two dimer active sites would disfavor binding at the second site, leading to slower reaction velocity and turnover for M567I.

Table 3. Substrate kinetic parameters of ALAS2 variants

	WT	**V562A**	**M567I***
Glycine			
V_{max} (U/mg)	12801 ± 333	28488 ±824	13653 ± 2545
K_M (mM)	10.1 ±0.8	23 ± 2	26 ± 17
k_{cat} (sec^{-1})	$1.75x10^{-3} \pm 5x10^{-5}$	$3.9x10^{-3} \pm 1x10^{-4}$	$1.45x10^{-3} \pm 5x10^{-5}$
k_{cat}/K_M ($sec^{-1}M^{-1}$)	0.173	0.169	0.056
Succinyl-CoA			

V_{max} (U/mg)	14929 ± 384	26422±1092	9041 ± 329
K_M (μM)	108 ± 8	272 ± 26	41 ± 5
k_{cat} (sec^{-1})	$2.040x10^{-3} \pm 5x10^{-6}$	$3.6x10^{-3} \pm 1x10^{-4}$	$1.16x10^{-3} \pm 2x10^{-5}$
k_{cat}/K_M ($sec^{-1}M^{-1}$)	18.9	13.2	28.3

*Allosteric sigmoidal fit: Glycine n_h=0.7 ± 0.1; succinyl-CoA n_h=0.78 ± 0.07

2.3 Discussion

Models

Together, the data identify that enzyme function can be impaired in more than one way. For example, M567I shows negative cooperativity of binding for glycine and succinyl-CoA substrates. M567I has decreased enzymatic activity and catalytic efficiency compared to WT, and this can be attributed to negative cooperativity of binding of both substrates. In contrast, the V562A variant has a defect in binding affinity to succinyl-CoA. Although V562A has enhanced enzymatic activity at saturating conditions, this defect in succinyl-CoA binding reduces catalytic efficiency. This is the first molecular explanation detailing the basis for reduced enzyme function in these XLSA variants.

PLP-Binding

The difference in PLP tautomerization for V562A and total PLP bound for M567I suggests that mild perturbations in the C-terminal extension have a profound impact on the enzyme. The PLP-binding pocket is located at the core of the enzyme near the dimer interface (**Figure 3**). The Ct-ext is solvent exposed and wrapped along the outer surface of the enzyme (**Figure 3**). When considering how Met567 maintains PLP in WT versus how Ile567 disrupts PLP in the mutant, I propose that this shift affects the propensity of the Ct-ext to wrap around the outer region of the structure. Computational models derived from programs such as AlphaFold Multimer predict that this region of the structure swings out and folds among the other Ct-ext residues (Hunter & Ferreira, 2022; Taylor, Ayres-Galhardo, & Brown, 2024), whereas the crystal structure captured this region wrapped around the outer surface. So, it is possible that this region exists in both states. Perhaps, shifting from Met567 to Ile567 causes the AlphaFold model to be more preferred, which would expose the PLP-binding pocket and allow PLP to dissociate more readily, thus resulting in lower total PLP bound for M567I.

I found that V562A has a higher percentage (68%) of PLP bound in the “active” state compared to WT and M567I (54%) (**Figure 10**). V562A has higher enzymatic activity compared to WT and M567I, which was

consistent with previous studies. The enhanced enzymatic activity could be explained by the propensity of PLP to favor the "active" state for V562A. One possible explanation for the effect on PLP tautomerization in V562A could be explained by increased flexibility resulting from Val562 changing to Ala562. Increased flexibility may allow for higher amounts of solvent accessibility which would hydrolyze the substituted aldimine (inactive) to the ketoenamine (active). This data once again highlights how mutations in the Ct-ext can have a vast impact on enzyme characteristics.

Protein Stability Compared to Cellular Half-Life

One detrimental effect that would impact ALAS2 function and contribute to XLSA is protein instability. Previous *in situ* studies monitored the half-life of V562A and M567I in cells and showed that V562A was destabilized, while M567I was stabilized compared to WT (Kadirvel et al., 2012). Based on this observation, I tested whether this phenomenon is consistent with the thermal stability of the mutant proteins. Consistent with protein half-life, I found that V562A was destabilized, and the stability of M567I was not significantly different than WT (**Figure 8**). The data here further supports the conclusion that V562A is a destabilized protein, despite having higher enzymatic activity. Destabilization may be an additional driving factor for the development of XLSA for V562A. This indicates that Val562 is an important residue for maintaining protein stability. The alteration of Val562 to Ala562 destabilizes the enzyme and results in a shorter half-life, highlighting the fidelity of the residues in the Ct-ext. Despite maintaining a critical salt bridge for enzymatic activity control, other residues in the Ct-ext are critical for maintaining enzymatic function.

Stabilization by PLP

Both of the mutants were stabilized from excess PLP to a similar degree as WT (~6°C increase with PLP). This shows that in addition to being critical for catalysis, PLP stabilizes the proteins. However, the mechanism for stabilization is still unknown. This data further validates the use of PLP-supplementation as treatment for both V562A and M567I. This suggests that the mechanism of PLP-treatment is based, in part, by increasing the stability of the mutant proteins.

Enzyme Kinetics

Based on these studies, a driving factor for impaired heme biosynthesis in the V562A variant of ALAS2 is a succinyl-CoA binding defect. Perhaps the decrease in substrate affinity coupled with a less stable enzyme results in the full manifestation of XLSA for V562A. Mutant ALAS2 enzymes harboring multiple defects is not uncommon. One mutation (R452C) had impaired succinyl-CoA affinity in addition to impaired cofactor affinity.

M567I had reduced specific activity compared to WT and V562A. This observation is consistent with a

previous study. Here, I discovered that although the K_M for glycine or succinyl-CoA may not explain impaired heme biosynthesis, there is significant impact on substrate cooperativity in M567I for glycine and succinyl-CoA. This likely leads to overall reduced reaction velocity and turnover. The defect in cooperativity coupled with decreased total PLP may work in conjunction to impair enzyme function and lead to XLSA for M567I. Parsing out all the enzymatic defects attributed to each XLSA mutation will be critical for the development of alternative treatments for XLSA, for which the current treatment responsiveness varies tremendously.

The enzymatic activity of M567I and V562A was unaffected by 10 μM PLP, similar to WT. Previous reports used 200 μM PLP to assess the effects of PLP on specific activity (Kadirvel et al., 2012). In the case of 200 μM PLP, both V562A and M567I exhibited increased specific activity. The difference observed here at 10μM may be explained by the reduced affinity for PLP in M567I and V562A, which has ~1.3 or 1.6-fold weaker affinity for PLP compared to WT, respectively. Although, 10 μM and 200 μM are both saturating PLP concentrations. Alternatively, PLP could be impacting ALAS2 by an unknown mechanism outside of binding at the active site, in which having higher exogenous PLP could enhance enzyme function, especially considering that PLP stabilized WT and the variants. This could also be an indicator for the need for higher dosages of PLP when considering oral PLP-supplementation. However, we recognize that metabolism, age, diet, and other factors contribute to an individual's responsiveness to PLP (Barton & Lee, 2006; Cazzola et al., 2002; Prades et al., 1995).

I speculate that the effect of PLP on specific activity or stability for mutant proteins could be an important component for predicting molecular defects in other ALAS2 variants. For M567I and V562A, PLP significantly stabilized the apo proteins, but it stabilized apo-M567I to the highest extent (**Figure 8**). I also concluded that holo-M567I had less PLP bound overall. Perhaps an apoenzyme's response to PLP is indicative of the nature of PLP-bound in its endogenous state. Additionally, the stability of holo and apo-V562A was impacted by exogenous PLP the least. Instead, V562A had a marked impairment in succinyl-CoA binding. Therefore, we believe that how specific activity and/or protein stability is affected by PLP *in vitro* could be used as a predictor for underlying molecular defects either stemming from PLP defects or stemming from other features such as substrate defects. Additionally, resistance to PLP effects on specific activity could indicate the need for higher amounts of PLP-supplementation. However, additional biochemical characterization for other XLSA mutants will be needed for verification.

Here, the enzymatic defects for the disease variants are multifold. I believe that the sensitivity of the Ct-ext to perturbations is highlighted by the multiple enzymatic deficiencies caused by M567I and V562A. In instances of XLSA, we have seen cases where multiple avenues of enzyme function are impaired (Bishop, Tchaikovskii, Hoffbrand, Fraser, & Margolis, 2012; Furuyama et al., 2006). Parsing out each of these will be critical for understanding the complete role of the Ct-ext. In addition, uncovering the molecular details of

dysfunction in other variants will be critical to move forward with treatments for XLSA beyond PLP-supplementation.

2.4 Materials and Methods

2.4.1 Protein Expression and Purification

DNA encoding hALAS2$_{54-587}$ was cloned into the pET28b vector in-frame with a ULP1 protease cleavable N-terminal His$_6$-SUMO tag and expressed in BL21-Codon Plus (DE3)-RIL cells (Agilent Technologies) in LB media with 50 µg/ml kanamycin. Site-directed mutagenesis (V562A and M567I) was carried out on hALAS2$_{54-587}$ using complementary primers (Supplementary Table 1) and confirmed by sequencing. All variants were transformed into BL21(DE3) RIL competent cells, and single-colony 50 mL LB inoculations were grown O/N at 37°C with 50 µg/ml kanamycin. The cultures were expanded by placing 10 mL of the O/N cultures into 1L LB with 50 µg/ml kanamycin. The cultures were grown at 37°C and induced at an OD_{600} of 0.6–0.8 with 0.5 mM IPTG for 4 h at 22°C. Cultures were then centrifuged and cell pellets stored at −80°C.

Cells were lysed with a high-pressure homogenizer and centrifuged at 30,000 × *g* for 20 min at 4°C. The clarified cell extract was incubated at 4°C with 5.0 mL of packed Ni-NTA resin pre-equilibrated with lysis buffer (25 mM HEPES pH 8.0, 400 mM NaCl, 100 mM KCl, 20 mM imidazole, 10% glycerol, 1.0 mM DTT). The column was washed with wash buffer (25 mM HEPES pH 8.0, 400 mM NaCl, 100 mM KCl, 20 mM imidazole, 10% glycerol, 1.0 mM DTT) until no visible protein was present according to Bio-Rad 1X protein dye. The protein was eluted with elution buffer (25 mM HEPES pH 8.0, 400 mM NaCl, 100 mM KCl, 250 mM imidazole, 10% glycerol, 1.0 mM DTT) until no residual protein eluted from the column according to Bio-Rad 1X protein dye. His$_6$-SUMO tag removal was carried out by overnight treatment at 4°C with ULP1 protease and dialyzed into dialysis buffer (25 mM HEPES pH 7.0, 150 mM KCl, 10% glycerol, 1.0 mM DTT). Following O/N dialysis, purification over Ni-NTA resin was executed. The eluant fractions were concentrated to 1-2 mL and applied to a Superdex 200 pg 16/600 column at 4°C pre-equilibrated in GF Buffer (25 mM HEPES pH 7.0, 150 mM KCl, 10% glycerol, 0.5 mM TCEP). Eluted protein fractions were pooled and concentrated to 10–20 mg mL^{-1}.

2.4.2 Enzymatic Activity Assays

Enzyme activity was measured with a discontinuous colorimetric activity assay as described by Shoolingin-Jordan et al. and Bailey et al. with adaptations. The reaction was initiated by combining 50 mM potassium phosphate (pH 7.0), 1 mM DTT, 10 mM $MgCl_2$, varying concentrations of glycine and succinyl-CoA, 10 µM PLP, and 100 nM (6 µg•mL^{-1}) purified enzyme (175 µL total). The reaction was incubated at 37 °C for 15 min

(previously optimized for linear ALA formation with enzyme concentration) and terminated by adding 100 µL of prechilled 10% trichloroacetic acid. The mixtures were centrifuged at 13,000 × *g* for 5 min to remove protein, and 240 µL of the resulting supernatant was added to 240 µL of 1 M sodium acetate, pH 4.6 followed by the addition of 20 µL acetylacetone (500 µL total). The samples were boiled at 100°C for 10 min to derivatize the ALA product. Samples were cooled for 15 min and three 100 µL aliquots per reaction (three technical replicates) were aliquoted in a 96-well clear-bottom plate and further derivatized with the addition of 100 µL modified Ehrlich's reagent.

The absorbance was monitored at 553 nm for 25 min with a microplate reader (Thermo Fisher Scientific). Absorbance values collected at the spectral maxima for each sample were converted to molar quantities of ALA using an extinction coefficient of 60,400 M^{-1} cm^{-1}. Kinetic parameters (V_{max}, K_m, and k_{cat}) were determined by combining 100mM glycine and either 300 µM (WT and M567I) or 1.25mM (V562A) succinyl-CoA for k_{cat}. For K_m, 5–100 mM glycine was combined with either 300 µM (WT and M567I) or 1.25 xmM succinyl-CoA (V562A) or 50–1000 µM succinyl-CoA was combined with 100 mM glycine. The resulting kinetic curves were fit with Michaelis–Menten or allosteric sigmoidal models in Prism GraphPad 9. Each data point represents the mean from three biological replicates with three technical replicates each, and the error bars represent the standard deviation. All kinetic values presented here are represented as mean ± SD. A one-way ANOVA was performed among the groups at maximum activity to determine significant differences. Significance was considered at $p < 0.05$ ($\alpha = 0.05$ for testing).

2.4.3 UV-Visible Absorbance and Fluorescence Spectroscopy

Absorbance profiles for $hALAS2_{54-587}$ and $hALAS2_{54-587}$ variants were obtained using a Molecular Devices SpectraMax M2 microplate reader with an ultra-micro quartz cuvette at room temperature. Absorbance scans were executed from 260 nm-500 nm with 40 µM protein in a buffer containing 25 mM Hepes, pH 7.0, 150 mM KCl, 10% glycerol, and 0.5 mM TCEP. Experimental scans were standardized by subtracting buffer-only spectra. The experiment was repeated for a total of three biological replicates. PLP ratios were calculated by taking absorbance units at either 326 nm for the inactive ratio or 424 nm for the active ratio and dividing by the sum of the total absorbance units of 326 nm and 424 nm. We performed a one-way ANOVA among the groups to determine significant differences. Significance was considered at $p < 0.05$ ($\alpha = 0.05$ for testing).

The fluorescence emission spectra of WT $hALAS2_{54-587}$ and $hALAS2_{54-587}$ variants were monitored in a black 384-well plate with a microplate reader (Thermo Fisher Scientific). Each protein was diluted with 1X PBS to 30 µM. PLP tautomers were visualized via excitation at 326 nm and 424 nm for the substituted aldimine and ketoenamine, respectively. The emission wavelength range was from 350 nm to 600 nm. The experiment was repeated for a total of three biological replicates. Experimental scans were standardized by subtracting

buffer-only spectra. Fluorescence spectra were quantitated with the fluorescence counts from the fluorescence emission spectra. We performed a one-way ANOVA among the groups to determine significant differences. Significance was considered at $p < 0.05$ ($\alpha = 0.05$ for testing).

2.4.4 PLP Binding Affinity

The apoenzymes of $hALAS2_{54-587}$ and $hALAS2_{54-587}$ variants were prepared by overnight incubation at 4°C of the cleaved, NiNTA purified dilate diluted 5x in stripping buffer (0.1 M potassium phosphate pH 7.5 +10% glycerol + 1 mM DTT) with 5 mM hydroxylamine HCl. This was followed by gel filtration with Superdex 200 pg 16/600 column pre-equilibrated in GF Buffer (25 mM HEPES pH 7.0, 150 mM KCl, 10% glycerol, 0.5 mM TCEP). Eluted protein fractions were pooled and concentrated to 10–20 mg mL^{-1}. For kinetic analyses, the apoenzyme preparations were titrated with increasing concentrations of PLP and measured for activity as described above. The resulting curves were fit with a Michaelis–Menten model and statistical significance was determined using a one-way ANOVA. All experiments were performed with a minimum of three biological replicates each with three technical replicates. The error bars represent the standard deviation. Values presented are the mean ± SD.

2.4.5 Inflection Temperatures

WT $hALAS2_{54-587}$ and $hALAS2_{54-587}$ variants were assayed for melting temperature with and without 10-fold excess PLP using nano differential scanning fluorimetry with NanoTemper Prometheus NT.Plex nanoDSF Protein Stability Analyzer. Proteins were diluted to 1 mg mL^{-1} (16.9 μM) in 25 mM Hepes, pH 7.0, 100 mM KCl, 10% glycerol, 0.5 mM TCEP and aspirated into Prometheus NT.48 Standard capillaries. Fluorescence intensities at 330 and 350 nm were measured from 25°C to 90°C with a ramp rate of 1°C min^{-1}. For PLP experiments, proteins were diluted to 1 mg mL^{-1} (16.9 μM) in buffer containing 25 mM Hepes, pH 7.0, 100 mM KCl, 10% glycerol, 0.5mM TCEP, 169 μM PLP and aspirated into Prometheus NT.48 Standard capillaries. PLP was added during protein dilution and incubated on ice for 10 min prior to aspirating. The inflection temperature (T_i) was determined for each variant with and without PLP. The experiment was repeated three times and an error was calculated based on the standard deviation. We performed a one-way ANOVA among the groups to determine significant differences. Significance was considered at $p < 0.05$ ($\alpha = 0.05$ for testing).

2.4.6 Circular Dichroism

Far-ultraviolet (UV) CD spectra were measured using a JASCO J-810 spectrometer continuously purged with nitrogen. The proteins were diluted to 8.0 μM (WT and M567I) or 6.0 μM (V562A) in 10 mM potassium phosphate pH 7.0, 100 mM KCl, and 0.5 mM TCEP and placed in a quartz cuvette with a 1.0 mm path length.

Spectra were recorded in continuous scanning mode at 25°C, from 250 nm to 190 nm at a scan speed of 20 nm/minute with a 0.5 nm data pitch and 1.0 nm bandwidth. Three spectra were accumulated and averaged for each sample. Experimental scans were standardized by subtracting buffer-only spectra.

CHAPTER 3

The Interaction of ALAS2 with SCS

3.1 Introduction

3.1.1 ALAS2 as a Regulator for Heme Biosynthesis

Aminolevulinic acid synthase (ALAS) is a PLP-dependent, mitochondrial enzyme that catalyzes the first and rate-limiting step of heme biosynthesis (Ferreira & Gong, 1995). ALAS catalyzes the condensation of glycine and succinyl-CoA to form aminolevulinic acid (ALA), the precursor for all biologically synthesized tetrapyrroles such as heme (Chiabrando et al., 2014; Hunter & Ferreira, 2009; Layer, 2020, 2021). This reaction is the committed step of heme biosynthesis. Thus, ALAS is considered the gatekeeper for heme biosynthesis (Hunter & Ferreira, 2011). ALAS exists as two isoforms in vertebrates (Bishop, 1990). ALAS1 is the ubiquitously expressed isoform, whereas ALAS2 is specific for erythroid cells (Bishop et al., 1990; Cox et al., 1992). ALAS2 synthesizes approximately 90% of total body hemoglobin for red blood cells (Wintrobe & Greer, 2004). In addition, ALAS1 cannot compensate for ALAS2 in its erythroid-specific cellular role (Nakajima et al., 1999). ALAS2 is regulated at the transcript level with a mitochondrial targeting sequence, iron response elements, and multiple transcription factors needing to coordinate for maximum expression (Melefors et al., 1993; Sadlon et al., 1999; Zhang et al., 2017). Additionally, ALAS2 is sensitive to mutations as seen in the >90 mutations that have been identified in the catalytic domain and C-terminal extension of ALAS2 that impact heme biosynthesis (Taylor & Brown, 2022). Even conservative missense mutations impact ALAS2 function and interferes with productive heme biosynthesis (Bishop, Tchaikovskii, Nazarenko, & Desnick, 2013; Taylor & Brown, 2022). The catalytic domain of ALAS2 houses the active site, and the C-terminal extension is an autoinhibitory region of the structure that is critical for maintaining normal enzyme activity (Bailey et al., 2020).

Mutations in ALAS2 can lead to loss of function, as in X-linked sideroblastic anemia, or gain of function, as in X-linked protoporphyria (Ashorobi & Chhabra, 2024; Balwani & Desnick, 1993). What has yet to be explored is how protein binding partners of ALAS2 can influence disease. One protein of interest is succinyl-CoA synthetase, which was identified as a binding partner for ALAS2 (Furuyama & Sassa, 2000). However, the biological relevance of its interaction with ALAS2 is unclear (**Figure 13**).

3.1.2 The Link Between the TCA Cycle and Heme Biosynthesis: Succinyl CoA Synthetase

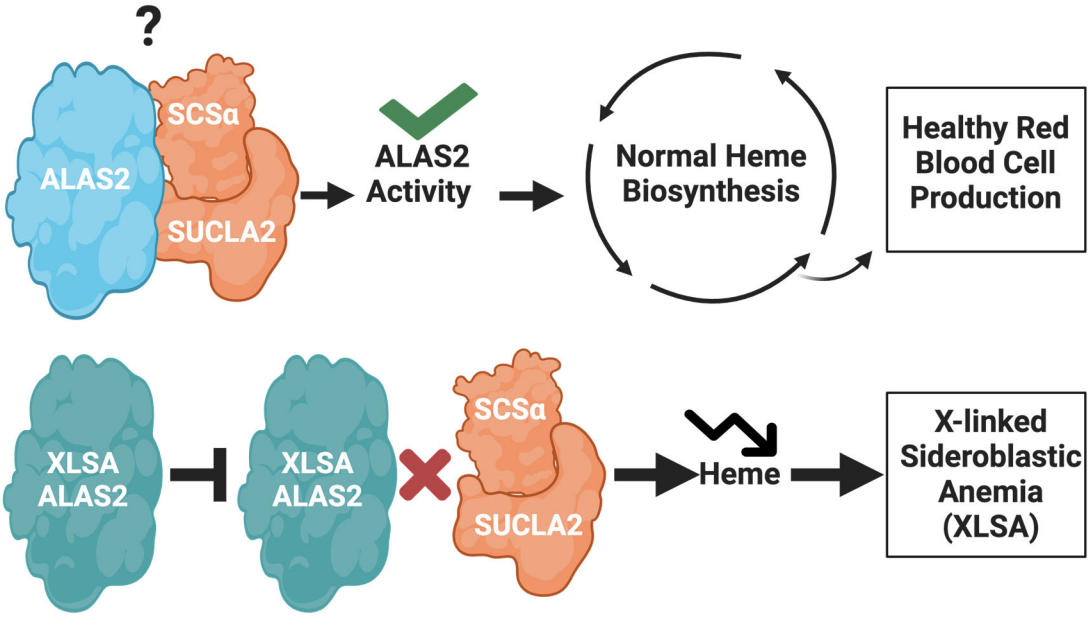

Figure 13. Biological question for this investigation. ALAS2 is represented in blue (wild-type) or teal (mutant) and SCS is represented in orange. ALAS2 binds SCS, but the biological relevance for the interaction in unknown. Additionally, certain XLSA disease mutations in ALAS2 disrupt assembly with SCS.

(Phillips, Aponte, French, Chess, & Balaban, 2009). Its role in the central TCA cycle makes it a key player in cellular metabolism. The conversion from succinyl-CoA to succinate by SCS is accompanied by the formation of a nucleotide triphosphate molecule (GTP or ATP). The specificity of forming GTP or ATP comes from the β subunit of SCS (Lambeth, Tews, Adkins, Frohlich, & Milavetz, 2004).

Bacterial SCS is composed of two αβ heterodimer molecules to form a heterotetramer (Wolodko, Fraser, James, & Bridger, 1994). Human SCS is made up of an α and β subunit to form an αβ heterodimer (Fraser, Hayakawa, Hume, Ryan, & Brownie, 2006; Huang & Fraser, 2022). The β subunit of SCS in humans is specific for either ATP or GTP depending on the tissue and energy requirements (Lambeth et al., 2004). SUCLA2 is ATP-specific and SUCLG2 is GTP-specific. Each subunit of SCS (SCSα, SUCLG2, or SUCLA2) is encoded by a separate gene (Lambeth et al., 2004).

Previous studies suggested that SCS is related to heme biosynthesis since its substrate, succinyl-CoA, is a substrate for the first step of heme biosynthesis catalyzed by ALAS (Burch et al., 2018). In a yeast-2-hybrid screen that probed mitochondrial binding partners for ALAS2, researchers identified the ATP-specific β subunit of SCS as a binding partner for hALAS2 (Furuyama & Sassa, 2000). They confirmed that the SCS heterodimer also interacted with ALAS2. This interaction is specific for ALAS2 and not ALAS1.

ALAS2 disease mutations leading to XLSA disrupt assembly with SCS and SUCLA2 (Bishop et al., 2012). Based on the disruption of complex formation from XLSA mutants and the specificity of SCS binding to the erythroid specific isoform of ALAS, SCS is thought to play an important role for developing red blood cells. However, the molecular details or complete biological understanding of the interaction remains to be uncovered (**Figure 13**). The four XLSA mutations that disrupt assembly with SCS are D190V, M567I, M567V, and S568G. Besides D190V, the mutations reside in the 44 amino acid critical C-terminal extension of ALAS2. I propose that the localization of the mutations to the C-terminal extension suggests a putative ALAS2 binding site for SCS. In this study, I have investigated the interaction between ALAS2 and SCS to uncover the molecular details of the interaction. Dissecting the interaction of ALAS2 and SCS will unveil the details necessary to understand role of SCS on ALAS2 function and heme biosynthesis.

3.2 Results

3.2.1 ALAS2 has a Weak Interaction with SCS and a Strong Affinity for SUCLA2

3.2.1.1 Microscale Thermophoresis

To characterize the binding of ALAS2 and either SCS or SUCLA2, I used microscale thermophoresis to measure the binding affinities for the protein complexes. The literature reveals that ALAS2 interacts with both SCS and SUCLA2 (Bishop et al., 2012). However, neither the strength of the interaction, nor the

molecular details of the interaction have been elucidated. Thus, I employed binding characterization for both protein binding partners. I found that ALAS2 binds SCS with a low micromolar affinity compared to nanomolar affinity for SUCLA2. The K_D value between ALAS2 and SCS was 10.5 ± 9 μM, whereas the K_D value between ALAS2 and SUCLA2 was 37.9 ± 13 nM (**Figure 14**). This result suggests that the α subunit of the SCS heterodimer may weaken the interaction between ALAS2 and SCS compared to ALAS2 and SUCLA2 alone. Thus, additional biophysical characterization was necessary.

3.2.2 Orthogonal Approaches to Characterize the ALAS2-SCS/SUCLA2 Protein Complexes

3.2.2.1 Affinity Pulldowns

I was curious if SCSα would interfere with complex formation between ALAS2 and SCS compared to ALAS2 and SUCLA2. To probe the interaction, I immobilized hexahistidine-tagged ALAS2 on NiNTA resin and incubated either SCS heterodimer or SUCLA2 with the immobilized protein resin. The proteins were eluted with 250 mM imidazole and the resulting eluant was analyzed with SDS-PAGE. The results indicated that His-ALAS2 did not complex with SCS nor SUCLA2 under the conditions tested (**Figure 15**). BSA was used as a negative control. The pI of the ALAS2-SUCLA2 complex is 6.65, and the pI of the ALAS2-SCS complex is 7.6. This experiment was repeated at two different pH values to ensure that pH was not interfering with complex formation (**Figure 15 A, B**). The inverse experiments with immobilized SCS or SUCLA2 were executed and yielded the same result (**Figure AIII**). Additionally, succinyl-CoA was included as a potential necessary component for complex formation, but the result was unchanged (**Figure AIII**).

3.2.2.2 Size Exclusion Chromatography Suggests that SUCLA2 is Viscid

I was unable to form a complex between His-ALAS2 and SCS or SUCLA2. I hypothesized that the N-terminal hexahistidine tag or column immobilization interfered with complex formation. Therefore, I implemented another binding approach to recapitulate the ALAS2-SCS/ALAS2-SUCLA2 complex. I utilized size exclusion chromatography (SEC) to confirm the complex between ALAS2 and SUCLA2, a nanomolar affinity interaction. I anticipated the interaction between ALAS2 and SCS to not be favorable for SEC. SEC is a technique in which a physical medium is used to separate molecules by size. Typically, weak interactors will not remain bound through the column.

As expected, ALAS2 and SCS eluted as separate species (**Figure 16A**) suggesting that they do not form a stable complex able to withstand SEC. Upon analysis of a 1:1 molar ratio for SUCLA2 to ALAS2, a monodispersed peak and SDS-PAGE analysis suggested that SUCLA2 coeluted with ALAS2 (**Figure 16B**).

A.

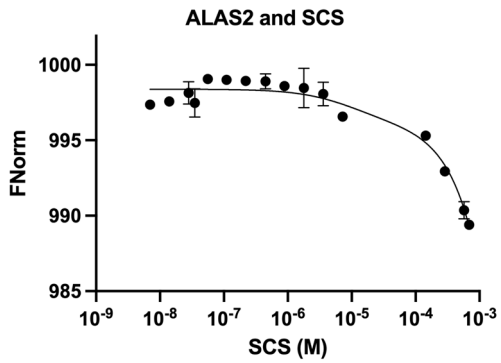

B.

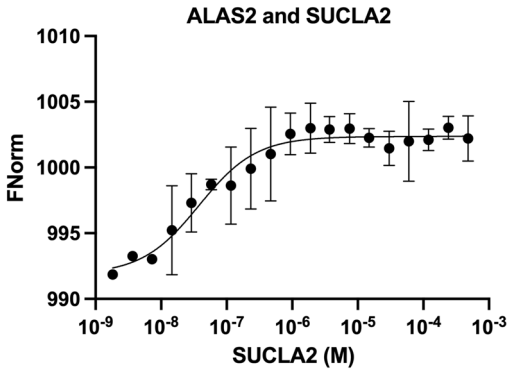

Figure 14. Binding affinity between ALAS2 and SCS is weaker than ALAS2 and SUCLA2. A) ALAS2-SCS binding curve from microscale thermophoresis (MST) using Alexa Fluor 488-labeled ALAS2 and titration of SCS. Curve represents three technical replicates. Binding affinity was obtained using one-site total binding model in Prism (GraphPad). K_D for ALAS2 and SCS is 10.5 μM ± 9 μM. B) ALAS2-SUCLA2 binding curve from microscale thermophoresis (MST) using Alexa Fluor 488-labeled ALAS2 and titration of SUCLA2. Curve represents three technical replicates. Binding affinity was obtained using one-site total binding model in Prism (GraphPad). K_D for ALAS2 and SUCLA2 is 37.9 nM ± 13 nM.

A.

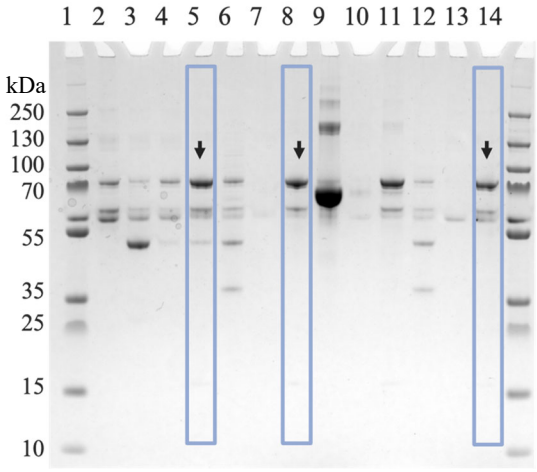

B.

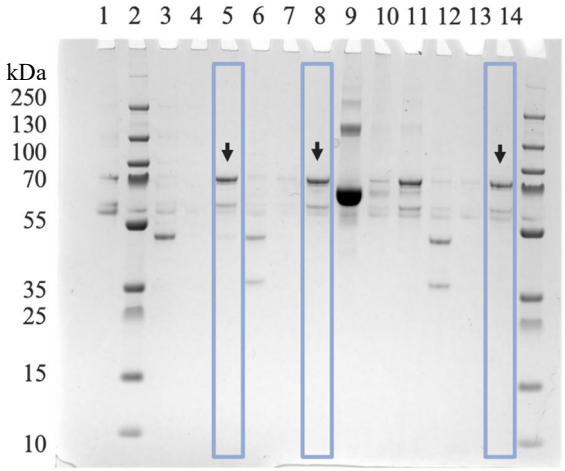

Figure 15. Affinity pulldown with His-ALAS2 did not isolate SCS or SUCLA2. A) SDS-PAGE analysis of His-tagged ALAS2 (71 kDa) immobilized to NiNTA resin with SCS (36 kDa and 49 kDa) and SUCLA2 (49 kDa) at pH 7.0. Elution lanes are noted in blue and His-ALAS2 is shown under each arrow. *Lane 1:* molecular weight marker*; lane 2:* His-ALAS2 flow-through after NiNTA incubation*; *lane 3:* SUCLA2 flow-through*; lane 4:* SUCLA2 wash*; lane 5:* elution from which SUCLA2 was loaded onto His-ALAS2 bound resin*; lane 6:* SCS flow-through*; lane 7:* SCS wash*; lane 8:* elution from which SCS was loaded onto His-ALAS2 bound resin; *lane 9*: BSA flow-through; *lane 10*: BSA wash*; lane 11:* elution from which BSA was loaded onto His-ALAS2 bound resin*; lane 12:* SCS flow-through**; *lane 13*: SCS wash*; lane 14:* elution from which SCS was loaded onto His-ALAS2 bound resin. B) SDS-PAGE analysis of His-tagged ALAS2 (71 kDa) immobilized to NiNTA resin with SCS (36 kDa and 49 kDa) and SULCA2 (49 kDa) at pH 8.2. *Lane 1:* His-ALAS2 flow-through after NiNTA incubation**; lane 2:* molecular weight marker; *lane 3:* SUCLA2 flow-through*; lane 4:* SULCA2 wash*; lane 5:* elution from which SUCLA2 was loaded onto His-ALAS2 bound resin*; lane 6:* SCS flow-through*; lane 7:* SCS wash*; lane 8:* elution from which SCS was loaded onto His-ALAS2 bound resin; *lane 9*: BSA flow-through; *lane 10*: BSA wash*; lane 11:* elution from which BSA was loaded onto His-ALAS2 bound resin*; lane 12:* SCS flow-through**; *lane 13*: SCS wash*; lane 14:* elution from which SCS was loaded onto His-ALAS2 bound resin.
*The two bands seen with His-ALAS2 correspond to the two populations of His-ALAS2 that were observed during purification.
**Two separate SCS preps were used to validate result.

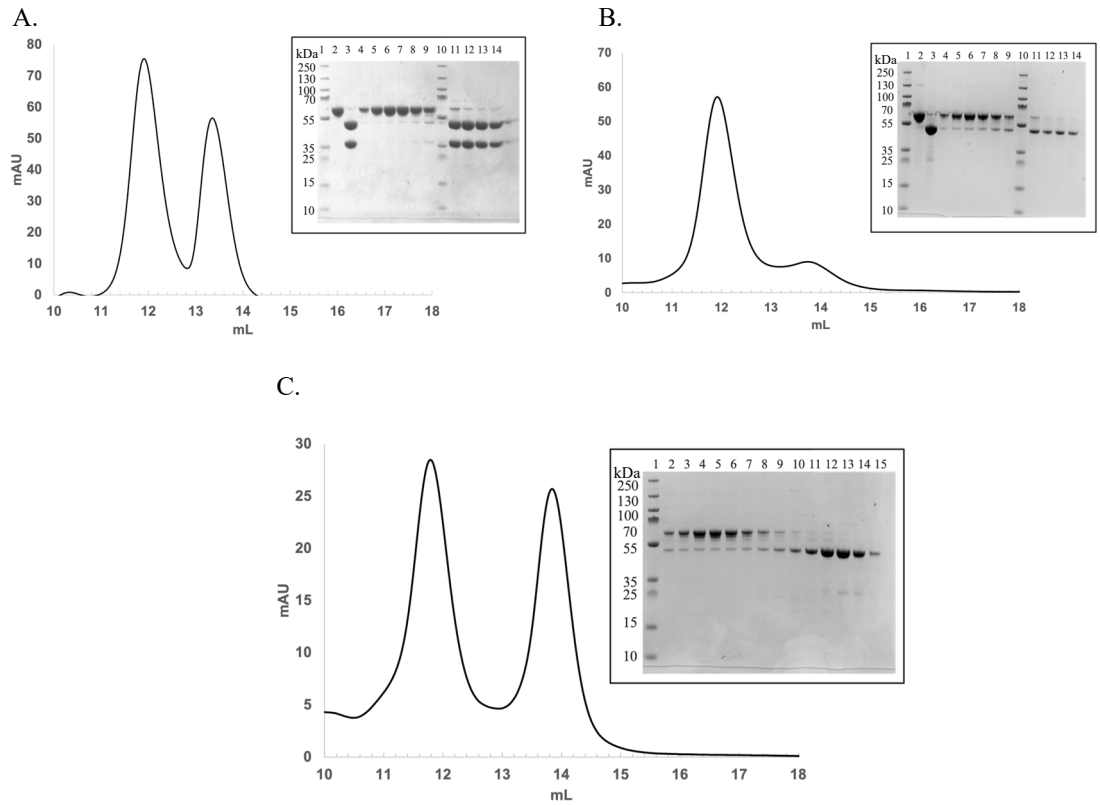

Figure 16. Effects of size exclusion chromatography on the binding of ALAS2 with SCS and SUCLA2. A) Chromatogram of 1:1 molar ratio of ALAS2 and SCS. Peak fractions were analyzed with SDS-PAGE (inset). SDS-PAGE analysis from 11.40 mL-14.15 mL of ALAS2 (59 kDa) and SCS (36 kDa and 49 kDa) in 0.25 mL fractions. *Lane 1:* molecular weight marker*; lane 2:* ALAS2 standard; *lane 3:* SCS standard*; lanes 4-9:* 11.40 mL-12.65 mL in 0.25 mL fractions*; lane 10*: molecular weight marker*; lanes 11-14:* 13.40 mL-14.15 mL in 0.25 mL fractions. B) SEC chromatogram of 1:1 molar ratio of ALAS2 and SUCLA2. Peaks fractions were analyzed with SDS-PAGE (inset). SDS-PAGE analysis from 11.15 mL-14.40 mL of ALAS2 (59 kDa) and SUCLA2 (49 kDa) in 0.25 mL fractions. *Lane 1:* molecular weight marker*; lane 2:* ALAS2 standard; *lane 3:* SUCLA2 standard*; lanes 4-9:* 11.15 mL-12.40 mL in 0.25 mL fractions*; lane 10*: molecular weight marker*; lanes 11-14:* 13.65 mL-14.40 mL in 0.25 mL fractions C) GF chromatogram of 1:2 molar ratio of ALAS2 and SUCLA2. Peaks fractions were analyzed with SDS-PAGE (inset). SDS-PAGE analysis from 10.65 mL-13.90 mL in 0.25 mL fractions containing ALAS2 (59 kDa) and SUCLA2 (49 kDa). *Lane 1:* molecular weight marker*; lane 2:* 10.65 mL; *lane 3:* 10.90 mL*; lane 4:* 11.15 mL*; lane 5:* 11.40 mL*; lane 6:* 11.65 mL*; lane 7:* 11.90 mL; *lane 8:* 12.15 mL; *lane 9*: 12.40 mL; *lane 10*: 12.65 mL*; lane 11:* 12.90 mL*; lane 12:* 13.15 mL *lane 13*: 13.40 mL*; lane 14:* 13.65 mL; *lane15:* 13.90 mL.

Shockingly, ALAS2 and SUCLA2 eluted as separate species when in a 2:1 molar ratio for SUCLA2 to ALAS2, as seen by the presence of two monodisperse peaks (**Figure 16C**). Interestingly, upon analysis of the early fractions in the 2:1 molar ratio experiment, both ALAS2 and SUCLA2 are present. This may be indicative of a large multimeric species forming between ALAS2 and SUCLA2. This may be because SUCLA2 is viscid or because of the nature of the interaction (**Figure 17A**). Based on the conflicting data from the different molar ratios of SUCLA2 to ALAS2, I next asked whether SUCLA2 would coelute with two mutant ALAS2 proteins that inhibit binding to SUCLA2 (Bishop et al., 2012). The mutants were M567I and S568G. Using these mutants as negative controls, I observed that there were trace amounts of SUCLA2 present in the fractions of the mutants (**Figure 17B**). The data reveal that although SUCLA2 does not bind to these mutants in the previous study, SUCLA2 elutes with WT and the mutant proteins during SEC. This data also suggests that a false positive could have occurred with the 1:1 molar ratio analysis between WT and SUCLA2. Based on these data, I propose that non-specific interactions occur with SUCLA2 through the protein surface that is typically not biologically exposed. When SCS exists as the biologically relevant heterodimer, the surface is typically abrogated by SUCLA2 binding to SCSα. Here, I have observed SUCLA2 coeluting with various binding partners in SEC regardless of its true binding character.

3.2.2.3 Native Gel Electrophoresis Shows Individual Subunits of ALAS2-SUCLA2 Complex

As an additional approach to capture the protein complex, I utilized native gel electrophoresis. By using non-reducing, non-denaturing conditions, I was striving to observe both subunits of the ALAS2- SUCLA2 complex migrate as one complex. This would further support the hypothesis that the purified proteins interact, as seen with MST binding curves. Curiously, ALAS2 and SUCLA2 migrated as individual subunits during native gel electrophoresis (**Figure 18**). Although native electrophoresis should preserve the noncovalent interactions between ALAS2 and SUCLA2, the two subunits of the complex did not withstand migration through the native gel. It may be important to consider that an additional nonprotein component is important and necessary for strengthening the interaction. Without the additional component, ALAS2 and either SCS or SUCLA2 interact in a way that is unable to withstand typical biophysical analysis.

3.2.3 Negative Stain Transmission Electron Microscopy of ALAS2 and SUCLA2 Reveal Monodispersed Particles

I took a structural approach to characterize the binding between ALAS2 and SCS or SUCLA2. Initially, I used X-ray crystallography to visualize the ALAS2-SCS complex. However, after analysis of the X-ray diffraction data from the protein crystals, I determined that the protein crystals contained only SCS. I transitioned to negative stain electron microscopy in preparation for cryogenic electron microscopy (Cryo-EM). Because ALAS2 had a stronger binding affinity for SUCLA2, I prepared negative stain grids with ALAS2 and

A.

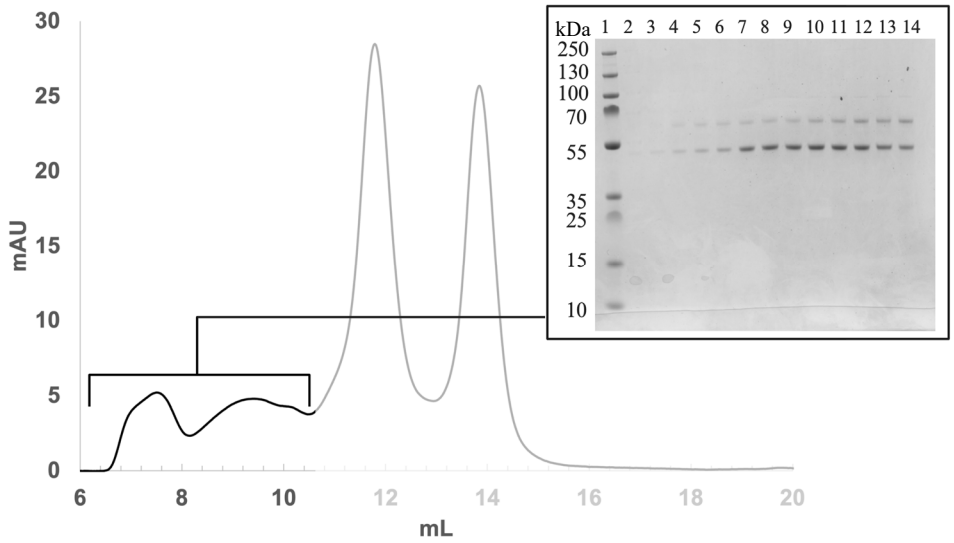

B.

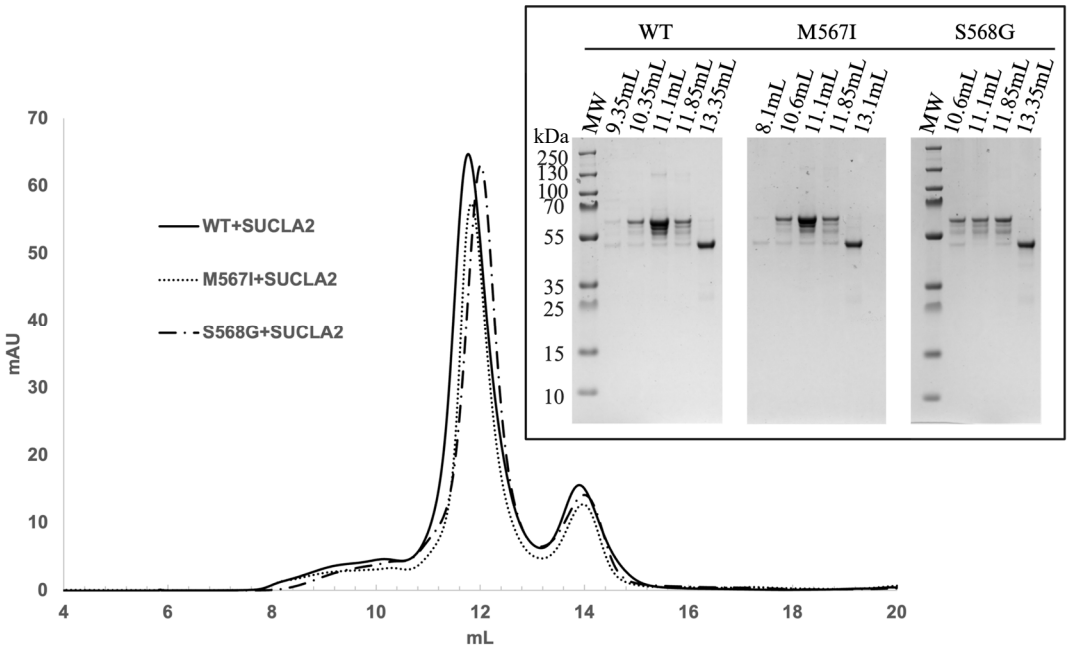

Figure 17. Size exclusion chromatography captures multimeric species containing ALAS2 and SUCLA2 and ALAS2 mutants coelute with SUCLA2. A) Chromatogram of 1:2 molar ratio of ALAS2 and SUCLA2 (**Figure 16B**) has region of obscurity from 6.00 mL-10.00 mL. Region fractions were analyzed with SDS-PAGE (inset). SDS-PAGE analysis from 6.65 mL-9.90 mL in 0.25mL fractions containing ALAS2 (59 kDa) and SUCLA2 (49 kDa). *Lane 1:* molecular weight marker*; lane 2:* 6.65 mL; *lane 3:* 6.90 mL*; lane 4:* 7.15 mL*; lane 5:* 7.40 mL*; lane 6:* 7.65 mL*; lane 7:* 7.90 mL; *lane 8:* 8.15 mL; *lane 9*: 8.40 mL; *lane 10*: 8.65 mL*; lane 11:* 8.90 mL*; lane 12:* 9.15 mL *lane 13*: 9.40 mL*; lane 14:* 9.65 mL. B) Overlay of WT ALAS2 (solid line), M567I (dotted line), and S568G (dashed line) GF elution profiles after incubation with SUCLA2. Fractions from each experiment were analyzed with SDS-PAGE (inset). Lanes are labeled with the corresponding elution volume of the fraction. Fractions from first peak (12.00 mL) indicate the presence of both ALAS2 and SUCLA2, which are seen at 59 kDa and 45 kDa, respectively.

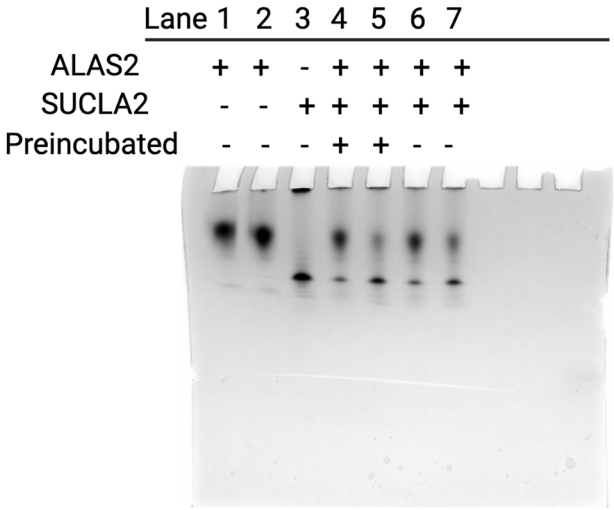

Figure 18. Native gel electrophoresis analysis illustrates ALAS2 and SUCLA2 migrate individually versus as a protein complex. Native-PAGE analysis of ALAS2 (118 kDa) with SUCLA2 (49 kDa). *Lane 1:* ALAS2; *lane 2:* ALAS2; *lane 3:* SUCLA2*; lane 4:* 2:1 molar ratio of ALAS2:SUCLA2 with 30 minute incubation; *lane 5:* 1:1 molar ratio of ALAS2:SUCLA2 with 30 minute incubation; *lane 6:* 2:1 molar ratio of ALAS2:SUCLA2 with no incubation*; lane 7:* 1:1 molar ratio of ALAS2:SUCLA2 with no incubation.

SUCLA2. Although SUCLA2 may be viscid, it is good practice to purify the sample prior to analysis to ensure that the sample of interest contains both ALAS2 and SUCLA2. Therefore, I incubated the ALAS2 and SUCLA2 complex and used SEC to isolate the complex. Taking fractions that contain both proteins of interest in a monodisperse peak, I determined the optimum conditions for preparing negative stain grids (**Figure 19**). The grids were used for collecting a dataset with negative stain transmission electron microscopy of the putative ALAS2-SUCLA2 complex. When the grids were screened, the particles were measuring ~80-100Ang. This was consistent with the combined size of ALAS2 and SUCLA2 as measured in Pymol.

3.3 Discussion

To gain a deeper understanding of the role for SCS as a binding partner of ALAS2, I discovered that the β subunit of SCS, or SUCLA2, binds ALAS2 with a stronger affinity than the heterodimer of SCS. However, whether SUCLA2 ever acts independently in the cell is unclear. The α and β subunits of SCS are encoded separately, but the functional unit exists as a heterodimer. Additionally, efforts to probe the complex through a variety of biophysical methods suggest that the ALAS2-SCS/SUCLA2 complex is either transient or requires the presence of an additional factor to form a stable complex. The initial discovery that ALAS2 binds SCS was conducted in a yeast host strain (Y190) and confirmed with immunoprecipitation from Chinese hamster ovary (CHO) cells (Furuyama & Sassa, 2000). Although my results do not dispute that ALAS2 binds SCS, one hypothesis to explain my data is that an additional component is necessary for stable complex formation. In a yeast expression system and CHO cells, there are cellular components present, such as cofactors, chaperones, or nucleotides, that would not be present with a purified protein. The need for an additional factor would be both opportunistic and problematic because it keeps the investigation of the interaction open in the field, but it also denotes the need for an extensive fishing expedition if the relevance of the interaction for heme biosynthesis is to be fully understood.

Affinity Pulldowns:

The other previous study of ALAS2 and SCS used maltose binding protein (MBP)-tagged proteins for affinity pull-downs to confirm the complex between ALAS2 and SCS or SUCLA2 (Bishop et al., 2012). In this study, the researchers found that certain XLSA mutations prevent binding to SCS and SUCLA2. Here, I was unable recapitulate the results from the study using His-tagged proteins (**Figure 15**, **AIII**). MBP is larger than an N-terminal hexahistidine tag. Outside of the tags, the purification techniques between the two studies were similar except that I utilized a second gel filtration purification step of the tagged proteins. The previous study isolated the bacterially expressed tagged proteins with affinity chromatography and did not include size exclusion chromatography to remove additional impurities. Instead, they implemented an ammonium acetate

A.

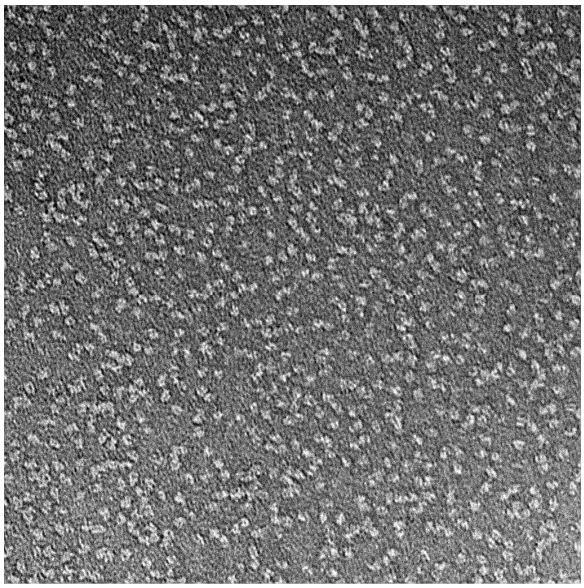

B.

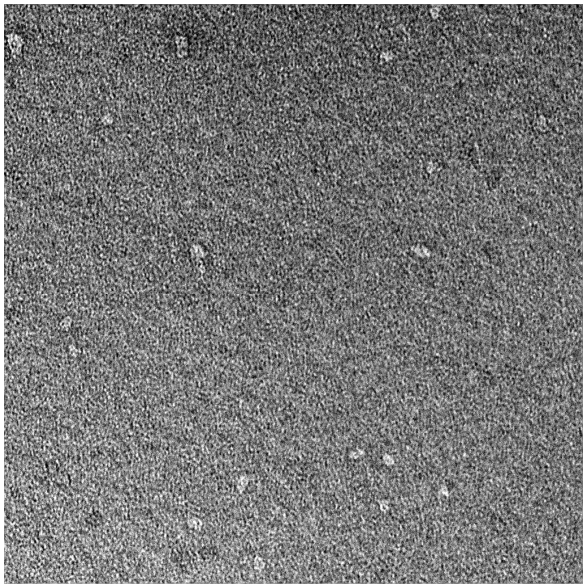

Figure 19. Representative transmission electron microscopy images illustrates monodispersed, homogenous particles of the putative ALAS2-SUCLA2 complex. TEM images of the ALAS2-SUCLA2 complex purified with chromatography and deposited on copper grids at A) 0.028 mg/mL or B) 0.010 mg/mL. Images were collected using the Morgani 268 with an AMT CCD 1k X 1k camera at 44,000x magnification, 100.0 kV.

precipitation step. Typically, working with purified proteins is favorable for biophysical characterization. In this case, the additional impurities may contain a critical factor for complex formation.

Chromatography and Native Gel Electrophoresis:

My findings highlight that ALAS2 and SUCLA2 coelute during size exclusion chromatography, but the results are ambiguous. The chromatogram and corresponding SDS-PAGE gel for ALAS2 and the SCS heterodimer show that the two proteins elute separately, as seen with two separate peaks and the corresponding SDS-PAGE gel (**Figure 16A**). The first peak (12.00 mL) and the second peak (13.50 mL) correspond to the elution volumes of the ALAS2 and SCS heterodimer standards. This result was expected based on the micromolar binding affinity measured with MST for ALAS2 and SCS. After analyzing the results from ALAS2 and SUCLA2, the data suggest that SUCLA2 forms nonspecific interactions and/or ALAS2 and SUCLA2 form a higher order multimeric complex. First, the 1:1 (ALAS2:SUCLA2) molar ratio chromatogram show a monodisperse peak indicative of one species. Comparing the chromatogram to the corresponding SDS-PAGE gel, ALAS2 and SUCLA2 are present in the peak with bands at 59 kDa for ALAS2 and 49 kDa for SUCLA2. Later eluent fractions of the peak only have SUCLA2 (49 kDa) (**Figure 16B**). Next, the 2:1 (SUCLA2:ALAS2) molar ratio chromatogram has two separate peaks, similar to the ALAS2 and SCS chromatogram (**Figure 16C**). The first peak is found at 11.90 mL and the second peak is present at 14.00 mL, which correspond to the elution volumes of the ALAS2 and SUCLA2 standards. However, comparing the 2:1 molar ratio chromatogram to the corresponding SDS-PAGE gel, ALAS2 and SUCLA2 are present in first peak with bands at 59 kDa for ALAS2 and 49 kDa for SUCLA2. With more SUCLA2 present relative to ALAS2, the amount of SUCLA2 in the first peak is lower compared to the second peak (14.0 mL) as seen by SDS-PAGE analysis (**Figure 16C**). I concluded that SUCLA2 coelutes with ALAS2, but the stoichiometry is low and the interaction is weak. Thus, SUCLA2 is in excess and travels separately too. The shoulder in Figure 14B from the 1:1 molar ratio experiment is SUCLA2, but the concentration was not high enough to appear as a clear peak. It was only when SUCLA2 was present at higher amounts (2:1 molar ratio) that the individual SUCLA2 peak emerged. Thus, SUCLA2 travels separately, but also coelutes with ALAS2. One explanation of the higher binding affinity observed for ALAS2 and SUCLA2 with MST may be explained with SUCLA2 forming nonspecific interactions in its monomeric form compared to the SCS heterodimer. SUCLA2 may have surface exposed regions that typically are abrogated by dimerization with SCSα. The next piece of data to suggest that SUCLA2 is a nonspecific binder was upon analysis of the abnormal region (6.0 mL-10.0 mL) from the 2:1 molar ratio experiment (**Figure 17A**). This region, which is in the void volume of the column, contained both ALAS2 and SUCLA2 (**Figure 17A**). The void volume is the volume where components that are too large to interact with the pores of the resin elute. This could be indicative of a multimeric complex between ALAS2 and SUCLA2. This result further highlights the need for dissecting the complete nature of the interaction in order to

understand the biological relevance of ALAS2 binding SCS.

Finally, M567I and S568G were used as negative controls for the chromatography experiments. M567I and S568G are ALAS2 XLSA disease mutations. M567V and S568G were previously reported to prevent binding to both SCS and SUCLA2 (Bishop et al., 2012). M567I is the disease variant of interest for this study, and it is the same residue that prevents binding to SCS and SUCLA2. Therefore, I implemented M567I as a negative control for binding to ALAS2. S568G is an XLSA mutation and was shown to prevent binding to SCS and SUCLA2. I used this variant as a bona fide negative control. For both M567I and S568G, trace amounts of SUCLA2 were present in the main peak fractions (11.85mL) similar to WT ALAS2 (**Figure 17B**). This data revealed that SUCLA2 coeluted with ALAS2 mutants that should have prevented ALAS2 complex formation. This data may indicate that during size exclusion chromatography, SUCLA2 forms nonspecific interactions that could be interpreted as a false positive for complex formation in the conditions tested here. These data illuminate the need for alternative methods to probe ALAS2 and SCS/SUCLA2.

Native gel electrophoresis was implemented to provide a gentler biophysical technique for analysis of the ALAS2-SUCLA2 complex. As seen in Figure 16, ALAS2 and SUCLA2 in either a 1:1 or 2:1 molar ratio did not travel as a complex during native gel electrophoresis. Despite the absence of detergents and the use of minimal salt conditions, the complex was not observed. This, combined with my previous biophysical data, indicates that complex formation between ALAS2 and SUCLA2 is not favorable with the purified proteins alone.

Negative-Stain Grids

Despite the inability to capture the ALAS2-SUCLA2 complex with affinity pull-down or native gel electrophoresis, I isolated a homogenous sample of ALAS2 and SUCLA2 from size exclusion chromatography and prepared TEM-grids for data collection. The images from grid screening indicated monodispersed particles (**Figure 19**). Electron microscopy (EM) data may reveal whether the peaks from size exclusion contain a stable complex between ALAS2 and SUCLA2 or if SUCLA2 is simply coeluting with ALAS2 in a random orientation regardless of the true binding character of the proteins. Understanding how SUCLA2 is interacting with ALAS2 in size exclusion will inform the nature of the interaction. Obtaining a preliminary EM structure will reveal the stoichiometry of the ALAS2 and SUCLA2 complex isolated from size exclusion chromatography. This, combined with the measured binding affinities, would be the first piece of biophysical data combined with structural data to characterize the binding of ALAS2 and SUCLA2.

Concluding Remarks

My findings reveal that ALAS2 and SUCLA2 coelute with size exclusion chromatography, but the additional

experiments conducted suggest that SUCLA2 may be a nonspecific binder. The inability to confidently isolate the complex using standard biophysical techniques lends the question of whether the purified proteins alone are sufficient to form a stable protein complex between ALAS2 and SCS or SUCLA2. Isolating proteins from their cellular context has its strengths and weaknesses. To further characterize the interaction of ALAS2 and SCS, it is imperative to identify what is necessary and sufficient for complex formation. It is also worth noting that there may be no evidence to investigate SUCLA2 over SCS with ALAS2 because as my results have shown, SUCLA2 can be an indiscriminate binding partner with ALAS2. SUCLA2 even coelutes with mutant proteins that inhibit binding to ALAS2 in another study. It is possible that SUCLA2, in its monomeric form, causes it to nonspecifically bind to other proteins. If SUCLA2 is not dimerized with SCSα, as in the SCS heterodimer, residues that would typically be abrogated by SCSα are exposed. Regardless, the data presented here highlight how additional factors or proteins can be critical for biological interactions. Before moving forward, the ALAS2-SCS complex needs further validation and additional investigation to understand the complete nature of the binding. Following validation and characterization, the role of the ALAS2 and SCS complex in heme biosynthesis or disease can be investigated. It is critical to define what is necessary for complex formation before moving forward.

3.4 Materials and Methods

3.4.1 Protein Expression and Purification

ALAS2

DNA encoding hALAS2$_{54\text{-}587}$ was cloned into the pET28b vector in-frame with a ULP1 protease cleavable N-terminal His$_6$-SUMO tag and expressed in BL21-Codon Plus (DE3)-RIL cells (Agilent Technologies) in LB media with 50 μg/ml kanamycin. Site-directed mutagenesis (V562A and M567I) was carried out on hALAS2$_{54\text{-}587}$ using complementary primers (Supplementary Table 1) and confirmed by sequencing. All variants were transformed into BL21(DE3) RIL competent cells and single-colony 50 mL LB inoculations were grown O/N at 37°C. The cultures were expanded by placing 10mL of the O/N cultures into 1L LB with 50 μg/ml kanamycin. The cultures were grown at 37°C and induced at an OD$_{600}$ of 0.6–0.8 with 0.5 mM IPTG for 4 h at 22°C. Cultures were then centrifuged and cell pellets stored at −80°C.

Cells were lysed with a high-pressure homogenizer and centrifuged at 30,000 × *g* for 20 min at 4°C. The clarified cell extract was incubated at 4°C with 5.0 mL of packed Ni-NTA resin pre-equilibrated with lysis buffer (25 mM HEPES pH 8.0, 400 mM NaCl, 100 mM KCl, 20 mM imidazole, 10% glycerol, 1.0 mM DTT). The column was washed with wash buffer (25 mM HEPES pH 8.0, 400 mM NaCl, 100 mM KCl, 20 mM

imidazole, 10% glycerol, 1.0 mM DTT) until no visible protein was present according to Bio-Rad 1X protein dye. The protein was eluted with elution buffer (25 mM HEPES pH 8.0, 400 mM NaCl, 100 mM KCl, 250 mM imidazole, 10% glycerol, 1.0mM DTT) until no residual protein eluted from the column according to Bio-Rad 1X protein dye. His_6-SUMO tag removal was carried out by overnight treatment at 4°C with ULP1 protease and dialyzed into dialysis buffer (25 mM HEPES pH 7.0, 150 mM KCl, 10% glycerol, 1.0 mM DTT). Following O/N dialysis, purification over Ni-NTA resin was executed. The eluant fractions were concentrated to 1-2 mL and applied to a Superdex 200 pg 16/600 column at 4°C pre-equilibrated in Size Exclusion Buffer (25 mM HEPES pH 7.0, 150 mM KCl, 10% glycerol, 0.5 mM TCEP). Eluted protein fractions were pooled and concentrated to 10–20 mg mL^{-1}.

SCS

DNA encoding $SUCLG1_{41-346}$ was cloned into the pOKD5 vector in-frame and $hSUCLA2_{53-463}$ was cloned into the pET28b vector in-frame with a ULP1 protease cleavable N-terminal His_6-SUMO tag and co-expressed in BL21-Codon Plus (DE3)-RIL cells (Agilent Technologies) in LB media with 50 µg/ml kanamycin and 100mg/ml ampicillin. Protein subunits were co-transformed into BL21(DE3) RIL competent cells and single-colony 50mL LB inoculations were grown O/N at 37°C with 50µg/ml kanamycin and 100 mg/ml ampicillin. The cultures were expanded by placing 10mL of the O/N cultures into 1L LB with 50 µg/ml kanamycin and 100mg/ml ampicillin. The cultures were grown at 37°C and induced at an OD_{600} of 0.6–0.8 with 0.5 mM IPTG for 4 h at 22°C. Cultures were then centrifuged and cell pellets stored at −80°C.

Cells were lysed with a high-pressure homogenizer and centrifuged at 30,000 × *g* for 20 min at 4°C. The clarified cell extract was incubated at 4°C with 5.0 mL of packed Ni-NTA resin pre-equilibrated with lysis buffer (50 mM Sodium Phosphate, pH 8.0, 500 mM NaCl, 1 mM DTT, 20 mM imidazole, pH 8.0, 10% glycerol). The column was washed with wash buffer (50 mM Sodium Phosphate, pH 8.0, 500 mM NaCl, 1 mM DTT, 20 mM imidazole, pH 8.0, 10% glycerol) until no visible protein was present according to Bio-Rad 1X protein dye. The protein was eluted with elution buffer (50mM Sodium Phosphate, pH 8.0, 500 mM NaCl, 1 mM DTT, 250 mM imidazole, pH 8.0, 10% glycerol) until no residual protein eluted from the column according to Bio-Rad 1X protein dye. His_6-SUMO tag removal was carried out by overnight treatment at room temperature with ULP1 protease and dialyzed into dialysis buffer (50 mM Sodium Phosphate, pH 8.0, 300 mM NaCl, 1 mM DTT, 10% glycerol). Following O/N dialysis, purification over Ni-NTA resin was executed. The eluant fractions were concentrated to 1-2 mL and applied to a Superdex 200 pg 16/600 column at 4°C pre-equilibrated in Size Exclusion Buffer (50 mM Sodium Phosphate, pH 8.0, 300 mM NaCl, 1 mM DTT, 10% glycerol). Eluted protein fractions were pooled and buffer exchanged into Storage Buffer (10 mM Tris, pH 8.0, 100 mM NaCl, 0.5 mM TCEP). Purified protein was concentrated to 10–20 mg mL^{-1} and flash

frozen for storage at -80°C.

SUCLA2 (SCSβ)

DNA encoding hSUCLA2$_{53-463}$ was cloned into the pET28b vector in-frame with a ULP1 protease cleavable N-terminal His$_6$-SUMO tag and expressed in BL21-Codon Plus (DE3)-RIL cells (Agilent Technologies) in LB media with 50 µg/ml kanamycin. Construct was transformed into BL21(DE3) RIL competent cells and single-colony 50 mL LB inoculations were grown O/N at 37°C with 50 µg/ml kanamycin. The cultures were expanded by placing 10 mL of the O/N cultures into 1L LB with 50 µg/ml kanamycin. The cultures were grown at 37°C and induced at an OD_{600} of 0.6–0.8 with 0.5 mM IPTG for 4 h at 22°C. Cultures were then centrifuged and cell pellets stored at −80°C.

Cells were lysed with a high-pressure homogenizer and centrifuged at 30,000 × *g* for 20 min at 4°C. The clarified cell extract was incubated at 4°C with 5.0 mL of packed Ni-NTA resin pre-equilibrated with lysis buffer (5 mM Imidazole, 50 mM Tris pH 8.0, 500 mM NaCl, 10% glycerol, 1.0 mM DTT) The column was washed with wash buffer (5 mM Imidazole, 50 mM Tris pH 8.0, 500 mM NaCl, 10% glycerol, 1.0 mM DTT) until no visible protein was present according to Bio-Rad 1X protein dye. The protein was eluted with elution buffer (250 mM Imidazole, 50 mM Tris pH 8.0, 500 mM NaCl, 10% glycerol, 1.0 mM DTT) until no residual protein eluted from the column according to Bio-Rad 1X protein dye. His$_6$-SUMO tag removal was carried out by overnight treatment at room temperature with ULP1 protease and dialyzed into dialysis buffer (50 mM Tris pH 8.0, 500 mM NaCl, 10% glycerol, 1.0 mM DTT). Following O/N dialysis, purification over Ni-NTA resin was executed. The eluant fractions were concentrated to 1-2 mL and applied to a Superdex 200 pg 16/600 column at 4°C pre-equilibrated in Size Exclusion Buffer (25 mM Tris pH 8.0, 200 mM NaCl, 10% glycerol, 0.5 mM TCEP). Eluted protein fractions were pooled and concentrated to 10–20 mg mL^{-1}.

3.4.2 Microscale Thermophoresis

hALAS2$_{54-587}$ was labeled with Alexa Fluor™ 488 C_5 Maleimide (Thermo Scientific) dye by dissolving 0.2-0.4 mg dye in 25 µL MST Buffer (20 mM HEPES, pH 8.2, 100 mM NaCl, 1 mM TCEP, 0.005% Tween-20) immediately prior to use for a dye stock solution. Dye sock solution was added to ALAS2 while stirring to produce approximately 25-30 moles of dye reagent per mole of protein. The reaction was allowed to proceed at room temperature for 1 hour, protected from light. The reaction solution was diluted to 400 µL and applied to an equilibrated Pierce™ Dye Removal Column (Thermo Scientific) and spinning 1000 x g, 2 min, 4°C to remove any unreacted thiol-reactive reagent. A serial 1:1 dilution was performed with either unlabeled SCS or SUCLA2 by transferring one volume of binding partner solution into an equal volume of MST buffer for 16 total dilutions. Labeled ALAS2 (ALAS2-488) (10 µL at 80 nM) was then added to each tube containing unlabeled protein binding partner (SCS or SUCLA2) for a total reaction volume of 20 µL. The reaction was

incubated at room temperature for 3 min before aspirating with Monolith™ NT.115 Standard glass capillaries. Samples were loaded and carried out in a NanoTemper Monolith™ NT.115 with the LED blue filter. Measurements were performed at 22 °C using 40% excitation and Medium MST power with a laser on-time of 20 s. All experiments were repeated three times for each measurement. Data analyses were performed using the NanoTemper analysis software. The dissociation constant (K_D) constants between a ALAS2 and SCS/SUCLA2 were calculated using a non-linear, one-site total binding model in Prism (GraphPad 9).

3.4.3 Native-PAGE

Samples were prepared by diluting ALAS2 or SUCLA2 to 20 µM with storge buffer (10 mM Tris pH 8.1, 0.1 M NaCl, 0.5 mM TCEP). For protein complexes, 30 µL of ALAS2 (20 µM) was combined with either 30 µL or 15 µL SUCLA2 (20 µM) for a 2:1 or 1:1 molar ratio, respectively. Protein complex samples were incubated on ice for 30 min. 15 µL of protein complex samples or individual protein samples were combined with 15 µL loading buffer (0.1 M Tris pH 8.0, 10% glycerol, 1 mM DTT, 0.1% bromophenol blue). 10µL (17 µmol) of each sample was loaded onto 4-16% Native-PAGE Bis Tris Gel (Invitrogen). Electrophoresis was run at 70V for 4hr, 50 min, chilled with running buffer (50 mM Tris pH 8.1, 50 mM boric acid, 1 mM DTT, 1 mM EDTA).

3.4.4 His-Trap Pulldown

Hexahistidine tagged-ALAS2 was diluted to 0.6 mg/mL with wash buffers (5 mM imidazole, 10 mM Tris pH 7.0, 0.1 M NaCl, 0.5 mM TCEP or 5 mM imidazole, 10 mM Tris pH 8.2, 0.1 M NaCl, 0.5 mM TCEP). 100 µL equilibrated NiNTA slurry (Qiagen) was combined with 100 µL His-ALAS2 (0.6 mg/mL) for pH 7.0 and pH 8.2. NiNTA, and His-ALAS2 was incubated 45 min at 4C before spinning 1500 x g, 2 min to pellet resin. Flow-through was removed. 100 µL each protein (0.15 mg/mL) (SCS, SUCLA2, or BSA) was added to His-ALAS2 resin or buffer plus resin. Proteins were incubated with His-ALAS2 immobilized resin for 15 min at room temperature. Samples were pelleted by spinning 1500 g, 2 min. Supernatant was removed. To wash the resin, 100 µL of designated wash buffer (pH 7.0 or pH 8.2) was added, and the resin was rocked for 2 min at room temperature. Samples were centrifuged, as above, to pellet the resin. This was repeated 3x for a total of 4 washes. Proteins were eluted by adding 200 µL designated elution buffer (250 mM imidazole, 10 mM Tris pH 7.0, 0.1 M NaCl, 0.5 mM TCEP or 250 mM imidazole, 10 mM Tris pH 8.2, 0.1 M NaCl, 0.5 mM TCEP). Elution buffer was incubated 5 min, 22°C. Eluent was collected by spinning 1500 x g, 2 min and removing the supernatant. Samples were analyzed with SDS-PAGE.

3.4.5 Size Exclusion Chromatography Analysis

Individual protein samples were prepared by obtaining 12 nmoles of purified ALAS2, SCS, or SUCLA2 and diluting to 200 µL with size exclusion buffer (10 mM Tris pH 8.2, 0.1 M NaCl, 0.5 mM TCEP). Filtered samples were applied to Superdex® 200 Increase 10/300 GL equilibrated in size exclusion buffer. Flow rate

was 0.5 mL/min. Fractions were collected in 0.250 mL volumes beginning at 6.0mL. For samples containing protein complexes, 11 nmoles of ALAS2 were combined with 11 nmoles of either SCS or SUCLA2 and incubated on ice for 30 min. For 2:1 molar ratio of SUCLA2:ALAS2, 12 nmoles SUCLA2 was combined with 6 nmoles ALAS2 and incubated on ice for 30 min. After incubation and filtering, protein complex samples were applied to equilibrated Superdex® 200 Increase 10/300 GL column. Fractions were collected in 0.250 mL volumes. Peak fractions were analyzed with SDS-PAGE analysis.

3.4.6 Negative-Stain Transmission Electron Microscopy

Grid Preparation:

Sample for grid was prepared by combining 11 nmol ALAS2 and 11 nmol SUCLA2 and diluting to 200 µL with size exclusion buffer (10 mM Tris pH 8.2, 0.1 M NaCl, 0.5 mM TCEP). Sample was incubated on ice for 30 min. Sample was applied to equilibrated Superdex 200 Increase 10/300 GL column. Fractions from main peak (11.4 mL elution volume) containing both ALAS2 and SUCLA2 according to SDS-PAGE were used for grid preparation. Sample was diluted to 0.028 mg/mL for application.

Carbon supported copper grids were charged with glow discharge system for 30 sec at 25 Amps. Once charged, 2.5 µL of 0.028 mg/mL or 0.010 mg/mL sample material was deposited on the grid and incubated for 30 sec before blotting residual sample with filter paper. Uranyl formate stain was applied to sample loaded grid and blotted with filter paper 2x. Finally, stain was added to sample loaded grid and allowed to incubate ~15 sec before blotting. Grid was air dried until imaged. Sample images were collected for screening on Morgani 268 with an AMT CCD 1k X 1k camera. Images were collected at 44,000x magnification, with 100 kV HT.

Electron Microscopy Data Set Collection:

Transmission electron microscopy dataset with conical tilt negative-stained images was collected on prepared grid (0.028 mg/mL) from *3.4.6* with the Tecnai F20 Cryo Electron Microscopy Microscope with 135,000x magnification and spot size: 5. Focus magnification was 100 kx with an exposure magnification of 62-80 kx.

CHAPTER 4

Discussion and Future Directions

4.1 Discussion

In Chapter II of this dissertation, I presented an in-depth study that isolated the enzymatic defects in two disease-causing variants of ALAS2, the erythroid-specific isoform of aminolevulinic acid synthase. The two variants, V562A and M567I, were identified in *ALAS2* by genetic testing after the male probands exhibited prolonged microcytic anemia, reduced hemoglobin levels, and systemic iron overload (Kadirvel et al., 2012). Ringed sideroblasts were observed in the patients' bone marrow cells establishing the diagnosis of sideroblastic anemia. Ringed sideroblasts are indicative of progressive iron overload in the mitochondria of bone marrow cells (Wintrobe & Greer, 2004). The X-chromosomal assignment of *ALAS2* and the deficiency in heme biosynthesis identifies this gene as the logical candidate underlying X-linked sideroblastic anemia (XLSA) (Cotter, Baumann, & Bishop, 1992; Cox et al., 1992). Screening for ALAS2 mutations typically occurs in a similar fashion as observed in the male probands that sparked this study. Individuals typically present with mild, moderate, or severe anemia with varying degrees of iron overload and low hemoglobin levels. Upon analysis, sideroblasts (>5%) are observed in the bone marrow cells. Following, a genetic screen is conducted to identify base changes in hematopoietic genes. After review, a mutation may be confirmed in ALAS2. To date, over 90 mutations have been identified in ALAS2 that lead to XLSA, and new XLSA mutations continue to be identified in ALAS2 every year (Ding et al., 2023; Taylor & Brown, 2022). Unfortunately, the molecular defect in ALAS2 has been dissected for only a few XLSA mutations. For example, the Y365C variant impairs pyridoxal-5'-phosphate (PLP) cofactor binding (Sankaran et al., 2015). Additionally, the R452C/H variants have reduced binding affinity for the succinyl-CoA substrate (Furuyama et al., 2006). Other XLSA variants F259C, D357V, and T388S/P are residues that directly interact with PLP according to the crystal structure, and thus, the underlying defect can be inferred as impacting PLP binding (Bailey et al., 2020). This leaves the majority of XLSA mutations without an underlying cause. Identifying the molecular defect underlying the disease is a critical component for 1) understanding the basis for disease and 2) the development of additional treatments for XLSA.

Pyridoxine, the precursor for PLP, supplementation is the standard treatment for XLSA (Ashorobi & Chhabra, 2024). Accompanied with pyridoxine supplementation can be phlebotomy and/or chelation to relieve the iron-overload effects. An unfortunate caveat of pyridoxine supplementation is that even patients with the same *ALAS2* mutation can have varying degrees of responsiveness to pyridoxine (Barton & Lee, 2006; Cazzola et al., 2002; Prades et al., 1995). Even so, the same mutation may be responsive to pyridoxine for one individual

and refractory for another individual. This has to do with factors such as metabolism, diet, and age (Barton & Lee, 2006; Cazzola et al., 2002; Prades et al., 1995). Further, an individual's responsiveness to pyridoxine may change as they age (C. S. Rose et al., 1976). An initial pyridoxine response does not warrant responsiveness for life and does not guarantee complete return to normal hemoglobin levels. For this reason, creative solutions beyond pyridoxine supplementation for XLSA treatment should be considered and explored. ALAS2 has a vast array of enzymatic characteristics to target. ALAS2 disease variants can have altered enzyme stability, structure, solubility, activity, kinetics, flexibility, cofactor binding, or ability to complex with other proteins. Here, we used a plethora of measurable characteristics of ALAS2 to parse out specifically what is underlying the enzymatic defect for V562A and M567I. A similar process could be utilized on the numerous XLSA mutations that have yet to be characterized. We found that V562A and M567I have different modes of impairing enzyme function.

V562A is destabilized compared to WT and had significantly reduced binding affinity for succinyl-CoA, the second substrate in the reaction mechanism for ALAS2 that forms aminolevulinic acid (ALA). Former cell-based studies in HEK293 cells measured the half-life of the mutant proteins and found that V562A has a shorter half-life than WT (Kadirvel et al., 2012). This coincides with our observation on thermal stability that V562A is destabilized compared to WT. In a biological context, a lower binding affinity for either substrate would disrupt normal execution of enzymatic function by impeding the amount of ALA formed. A cell does not have excessive amounts of glycine and succinyl-CoA substrates in the mitochondria. So, a reduced affinity for succinyl-CoA would be sensed by the cells requiring efficient function of the required enzyme. For ALAS2, developing red blood cells would bear the results of the defect because these cells require large amounts of heme production for hemoglobin. ALAS2 function is necessary for productive heme biosynthesis as it catalyzes the first and rate-limiting step of heme biosynthesis (Hunter & Ferreira, 2009, 2011; Stojanovski et al., 2019). An impediment in the reaction mechanism stemming from impaired succinyl-CoA binding likely impairs overall heme production for erythroid precursors, while iron continues to be transported to the mitochondria as normal. Thus, the development of XLSA ensues. The reduced ability to bind succinyl-CoA combined with a destabilized enzyme may have confounding effects in practice that result in severe consequences on the production of heme in people harboring the V562A mutation.

Using the same enzymatic analysis, we saw that M567I has a lower specific activity compared to WT under saturating substrate conditions. This result is consistent with a previous study that measured enzyme activity for this variant (Kadirvel et al., 2012). When considering M567I in the context of disease and treatment, we aimed to identify the underlying cause for reduced activity that leads to decreased heme production. As mentioned, there are many characteristics of ALAS2 that must be optimal for proper execution of heme biosynthesis. We wanted to determine 1) the underlying cause for lower activity and 2) any other enzymatic

defects at play that would provide insight into the onset of XLSA.

We found that for both glycine and succinyl-CoA substrates, M567I displays negative cooperativity in binding. This would indicate that the binding of substrate at one of the two dimer active sites would disfavor binding at the second site, leading to slower reaction velocity and turnover for M567I. Further, the k_{cat} for glycine was significantly diminished compared to WT. Unlike V562A, M567I has a similar thermal stability as WT, which suggests that the disease variant was not a destabilizing mutation. In reference to the previously mentioned cell-based study, M567I had a longer half-life than WT in HEK293 cells, further indicating that the mutation does not impact protein stability. One interesting observation was that M567I had less overall PLP bound per protein unit. Both V562A and M567I had slightly higher PLP binding constants compared to WT (1.6 and 1.3 fold increases, respectively). Despite a higher PLP binding constant for V562A, only M567I had less total PLP bound. It is unclear whether the amount of PLP bound for M567I contributes to its reduced activity or if the activity effects come solely from the substrate effects. However, the knowledge of both implications resulting from the M567I mutation sheds light on the combination of defects that can stem from one mutation in ALAS2. If another mutation were to cause the same enzymatic defects, it is possible that the subsequent tailored treatment would be successful on that mutation as well.

This is the first in-depth study to isolate the molecular defect underlying loss of function for these two disease variants. When considering additional treatments for the disease, it may not be sufficient information that an enzyme has lower activity. It is critical to provide complete characterization from all aspects of enzyme function to fully understand the mechanisms at play. One area where this study could benefit is to determine the 3-dimensional structure of the mutant enzymes. This would enable us to capture more molecular details of the effect of V562A and M567I mutations on ALAS2. Based on any structural implications, we would arrive at a more complete understanding of the basis underlying XLSA. For M567I, crystallizations screens were executed, and a promising starting place for future expansion was identified (**Figure AII**). Future structural studies that expand this result and determine the structure of V562A would be advantageous for furthering our understanding of XLSA derived from these disease variants.

When considering the molecular defects at play in XLSA from V562A and M567I, one avenue to be explored for treatment is pharmacological supplementation of either substrate. V562A caused a significant impairment in succinyl-CoA binding, and M567I had negative cooperativity of binding for both substrates as well as a diminished k_{cat} for glycine. Glycine supplementation was tested in a trial of 3 patients with a deficiency in the glycine transporter SLC25A38 but has not been utilized in targeting ALAS2 defects (LeBlanc et al., 2016). Likewise, therapeutically targeting succinyl-CoA has not been attempted for ALAS2 defects. Succinyl-CoA is known to self-hydrolyze (Trefely, Lovell, Snyder, & Wellen, 2020). Thus, the stability of succinyl-CoA

should be considered when implementing treatment.

4.2 Expanding Our XLSA Variant Investigation to Other Model Organisms

Future directions for this project are to continue our work in an erythroid-specific cell line. So far, cell-based studies have been conducted in HEK293 cells. Other cell lines that are more relevant to XLSA are available (Daniels et al., 2020). For example, HUDEP2 cells are an erythroid cell line that represent 'normal' erythroid cells, in that they produce functional hemoglobin, express erythroid-specific markers, and give rise to enucleated red blood cells after induction of differentiation. Further, HUDEP2 cells were utilized to model XLSA for two disease mutations (Kaneko et al., 2018; Ono et al., 2022). The researchers were successful in generating the mutant cell lines in HUDEP2 cells using CRISPR that generated iron-loaded ringed sideroblasts. Implementing this technology in the context of our study would allow us to monitor the ramifications of the mutations in the context of an erythroid cell. This would enable us to gain a wholistic picture of how the underlying dysfunction would impact an erythroid cell's ability to differentiate, produce hemoglobin, and isolate other disease-contributing factors. Additionally, the potential to test new therapeutics for XLSA could be realized in HUDEP2 XLSA mutant cell lines.

4.3 Additional Remarks

In Chapter III of this dissertation, I aimed to recapitulate a previous study that explored ALAS2 and its interaction with binding partner SUCLA2, the β subunit of succinyl-CoA synthetase (SCS). My goal was to characterize the nature of the interaction to understand the role that SUCLA2 plays on modulating ALAS2 function. Certain XLSA variants were previously reported to disrupt ALAS2 assembly with SUCLA2 (Bishop et al., 2012). Among these were M567V and S568G. I aimed to investigate specific XLSA variants that interfere with ALAS2 assembly with SUCLA2. Together, I aimed to uncover details of the ALAS2-SUCLA2 interaction that could be used to understand how ALAS2 is regulated or controlled by other protein binding partners. Unfortunately, I was unable to recapitulate the results of the previous study that used affinity pulldowns with either tagged ALAS2 or SCS and untagged ALAS2, SUCLA2, or SCS. Despite comprehensive attempts, I could not confidently capture the complex with affinity pulldowns. I implemented size exclusion chromatography to capture the complex, but this technique was met with inconclusive results between ALAS2 and SUCLA2 and SCS. Being the same impacted residue as M567V, I used M567I and S568G, a bona fide disrupter of the complex, as negative controls for complex formation with size exclusion chromatography. These variants showed similar elution profiles with SUCLA2 as WT ALAS2, which

contributed to the notion that an additional factor may be needed for stable complex formation in biophysical experiments and that SUCLA2 may bind proteins nonspecifically.

Despite this, I was able to determine the binding affinity constant for ALAS2 and SUCLA2 using microscale thermophoresis, which was in the mid nanomolar range (37.9 ± 13nM). I determined the binding affinity constant for ALAS2 and SCS and found that it was in the lower micromolar range (10.5 ± 9μM). This is the first report of the strength of the interaction between ALAS2 and either SUCLA2 or SCS. These binding affinities can be utilized when designing future experiments between ALAS2 and SCS/SUCLA2. I concluded that for biophysical techniques such as affinity pulldowns and size exclusion chromatography, there is likely an additional component necessary for stable complex formation. Before moving forward, additional work to identify what is necessary for stable complex formation must be completed.

4.4 Concluding Remarks

XLSA is classified as a rare disease in the United States. This is defined as impacting less than 200,000 people per year in the US (Abu-Zeinah & DeSancho, 2020). A consideration for this disease is that it manifests similarly to other rare anemias, such as thalassemia, which is characterized by smaller than normal red blood cells (microcytic anemia), reduced hemoglobin levels, and sometimes an enlarged liver or spleen (Thomas et al., 2023). These symptoms are consistent with the onset of XLSA. XLSA, as well as other hemopoietic disorders, need genetic testing for diagnosis. Without genetic testing, it is possible for XLSA to be mistaken for another anemia for which other common treatments, such as iron supplementation, would be detrimental (Ducamp & Fleming, 2019; Thomas et al., 2023). One unique aspect of XLSA is that it manifests as microcytic anemia in males and some females, but it can manifest as *macrocytic* anemia in certain females (Fujiwara et al., 2017; Sankaran et al., 2015). For this reason, diagnosis of the disorder in females can be inconclusive or inaccurate since diseases associated with macrocytic anemia are specific mitochondrial disorders, myelodysplastic syndromes, and megaloblastic anemia, for example (Ducamp & Fleming, 2019; Hariz & Bhattacharya, 2024; Nagao & Hirokawa, 2017). This further highlights the need for genetic testing when diagnosing a hematopoietic disorder such as XLSA.

4.5 Summary

In summary, I determined previously unknown molecular defects in the disease variants V562A and M567I in the erythroid-specific enzyme ALAS2 that underlies the rare blood disease X-linked sideroblastic anemia. I showed that using a comprehensive enzymatic analysis, I dissected the specific alteration in enzyme function that would adversely affect ALAS2 function in its cellular context. I discovered a greater need for additional

studies between ALAS2 and its binding partner SUCLA2 and find that the relationship between ALAS2 and SUCLA2 may be different than its relationship with SCS. These observations generate several avenues to be investigated in future studies of ALAS2 and XLSA that would add to our understanding of heme biosynthesis across all forms of life.

References

Abu-Zeinah, G., & DeSancho, M. T. (2020). Understanding Sideroblastic Anemia: An Overview of Genetics, Epidemiology, Pathophysiology and Current Therapeutic Options. *J Blood Med, 11*, 305-318. doi:10.2147/JBM.S232644

Ashorobi, D., & Chhabra, A. (2024). Sideroblastic Anemia. In *StatPearls*. Treasure Island (FL) ineligible companies. Disclosure: Anil Chhabra declares no relevant financial relationships with ineligible companies.

Astner, I., Schulze, J. O., van den Heuvel, J., Jahn, D., Schubert, W. D., & Heinz, D. W. (2005). Crystal structure of 5-aminolevulinate synthase, the first enzyme of heme biosynthesis, and its link to XLSA in humans. *EMBO J, 24*(18), 3166-3177. doi:10.1038/sj.emboj.7600792

Bailey, H. J., Bezerra, G. A., Marcero, J. R., Padhi, S., Foster, W. R., Rembeza, E., . . . Yue, W. W. (2020). Human aminolevulinate synthase structure reveals a eukaryotic-specific autoinhibitory loop regulating substrate binding and product release. *Nat Commun, 11*(1), 2813. doi:10.1038/s41467-020-16586-x

Balwani, M. (2019). Erythropoietic Protoporphyria and X-Linked Protoporphyria: pathophysiology, genetics, clinical manifestations, and management. *Mol Genet Metab, 128*(3), 298-303. doi:10.1016/j.ymgme.2019.01.020

Balwani, M., & Desnick, R. (1993). X-Linked Protoporphyria. In M. P. Adam, J. Feldman, G. M. Mirzaa, R. A. Pagon, S. E. Wallace, L. J. H. Bean, K. W. Gripp, & A. Amemiya (Eds.), *GeneReviews((R))*. Seattle (WA).

Barton, J. C., & Lee, P. L. (2006). Disparate phenotypic expression of ALAS2 R452H (nt 1407 G --> A) in two brothers, one with severe sideroblastic anemia and iron overload, hepatic cirrhosis, and hepatocellular carcinoma. *Blood Cells Mol Dis, 36*(3), 342-346. doi:10.1016/j.bcmd.2006.01.010

Bishop, D. F. (1990). Two different genes encode delta-aminolevulinate synthase in humans: nucleotide sequences of cDNAs for the housekeeping and erythroid genes. *Nucleic Acids Res, 18*(23), 7187-7188. doi:10.1093/nar/18.23.7187

Bishop, D. F., Henderson, A. S., & Astrin, K. H. (1990). Human delta-aminolevulinate synthase: assignment of the housekeeping gene to 3p21 and the erythroid-specific gene to the X chromosome. *Genomics, 7*(2), 207-214. doi:10.1016/0888-7543(90)90542-3

Bishop, D. F., Tchaikovskii, V., Hoffbrand, A. V., Fraser, M. E., & Margolis, S. (2012). X-linked sideroblastic anemia due to carboxyl-terminal ALAS2 mutations that cause loss of binding to the beta-subunit of succinyl-CoA synthetase (SUCLA2). *J Biol Chem, 287*(34), 28943-28955. doi:10.1074/jbc.M111.306423

Bishop, D. F., Tchaikovskii, V., Nazarenko, I., & Desnick, R. J. (2013). Molecular expression and characterization of erythroid-specific 5-aminolevulinate synthase gain-of-function mutations causing X-linked protoporphyria. *Mol Med, 19*, 18-25. doi:10.2119/molmed.2013.00003

Bottomley, S. S., May, B. K., Cox, T. C., Cotter, P. D., & Bishop, D. F. (1995). Molecular defects of erythroid 5-aminolevulinate synthase in X-linked sideroblastic anemia. *J Bioenerg Biomembr, 27*(2), 161-168. doi:10.1007/BF02110031

Brown, B. L., Kardon, J. R., Sauer, R. T., & Baker, T. A. (2018). Structure of the Mitochondrial Aminolevulinic Acid Synthase, a Key Heme Biosynthetic Enzyme. *Structure, 26*(4), 580-589 e584. doi:10.1016/j.str.2018.02.012

Burch, J. S., Marcero, J. R., Maschek, J. A., Cox, J. E., Jackson, L. K., Medlock, A. E., . . . Dailey, H. A., Jr. (2018). Glutamine via alpha-ketoglutarate dehydrogenase provides succinyl-CoA for heme synthesis during erythropoiesis. *Blood, 132*(10), 987-998. doi:10.1182/blood-2018-01-829036

Cao, H., Wang, J., He, L., Qi, Y., & Zhang, J. Z. (2019). DeepDDG: Predicting the Stability Change of Protein Point Mutations Using Neural Networks. *J Chem Inf Model, 59*(4), 1508-1514. doi:10.1021/acs.jcim.8b00697

Cazzola, M., May, A., Bergamaschi, G., Cerani, P., Ferrillo, S., & Bishop, D. F. (2002). Absent phenotypic expression of X-linked sideroblastic anemia in one of 2 brothers with a novel ALAS2 mutation. *Blood, 100*(12), 4236-4238. doi:10.1182/blood-2002-03-0685

Chiabrando, D., Mercurio, S., & Tolosano, E. (2014). Heme and erythropoieis: more than a structural role. *Haematologica, 99*(6), 973-983. doi:10.3324/haematol.2013.091991

Cotter, P. D., Baumann, M., & Bishop, D. F. (1992). Enzymatic defect in "X-linked" sideroblastic anemia: molecular evidence for erythroid delta-aminolevulinate synthase deficiency. *Proc Natl Acad Sci U S A, 89*(9), 4028-4032. doi:10.1073/pnas.89.9.4028

Cotter, P. D., Drabkin, H. A., Varkony, T., Smith, D. I., & Bishop, D. F. (1995). Assignment of the human

housekeeping delta-aminolevulinate synthase gene (ALAS1) to chromosome band 3p21.1 by PCR analysis of somatic cell hybrids. *Cytogenet Cell Genet, 69*(3-4), 207-208. doi:10.1159/000133964

Cotter, P. D., Rucknagel, D. L., & Bishop, D. F. (1994). X-linked sideroblastic anemia: identification of the mutation in the erythroid-specific delta-aminolevulinate synthase gene (ALAS2) in the original family described by Cooley. *Blood, 84*(11), 3915-3924. Retrieved from https://www.ncbi.nlm.nih.gov/pubmed/7949148

Cox, T. C., Bawden, M. J., Martin, A., & May, B. K. (1991). Human erythroid 5-aminolevulinate synthase: promoter analysis and identification of an iron-responsive element in the mRNA. *EMBO J, 10*(7), 1891-1902. Retrieved from https://www.ncbi.nlm.nih.gov/pubmed/2050125

Cox, T. C., Kozman, H. M., Raskind, W. H., May, B. K., & Mulley, J. C. (1992). Identification of a highly polymorphic marker within intron 7 of the ALAS2 gene and suggestion of at least two loci for X-linked sideroblastic anemia. *Hum Mol Genet, 1*(8), 639-641. doi:10.1093/hmg/1.8.639

Cui, Z., Zhu , Z., Zhang, J., Jiang, J., Liu, Y., Wang, Q., Hou, J., Qi, Q. (2021). Efficient 5-aminolevulinic acid production through reconstructing the metabolic pathway in SDH-deficient Yarrowia lipolytica. *Biochemical Engineering Journal, 174*.

Dailey, H. A., & Meissner, P. N. (2013). Erythroid heme biosynthesis and its disorders. *Cold Spring Harb Perspect Med, 3*(4), a011676. doi:10.1101/cshperspect.a011676

Daniels, D. E., Downes, D. J., Ferrer-Vicens, I., Ferguson, D. C. J., Singleton, B. K., Wilson, M. C., . . . Frayne, J. (2020). Comparing the two leading erythroid lines BEL-A and HUDEP-2. *Haematologica, 105*(8), e389-e394. doi:10.3324/haematol.2019.229211

de Gennes, C., Lamoril, J., Borgel, A., Boi, C., Yao, R., Boileau, C., & Tchernitchko, D. (2022). Severe iron overload in a woman with homeostatic iron regulator (HFE) and a novel 5'-aminolevulinate synthase 2 (ALAS2) mutations: interactions of multiple genetic determinants. *Br J Haematol, 196*(2), e17-e20. doi:10.1111/bjh.17810

Ding, Y., Yang, K., Liu, X., Xiao, J., Li, W., & Zhong, H. (2023). A Novel ALAS2 Mutation Causes Congenital Sideroblastic Anemia. *Mediterr J Hematol Infect Dis, 15*(1), e2023062. doi:10.4084/MJHID.2023.062

Donker, A. E., Raymakers, R. A., Nieuwenhuis, H. K., Coenen, M. J., Janssen, M. C., MacKenzie, M. A., . . . Swinkels, D. W. (2014). X-linked sideroblastic anaemia due to ALAS(2) mutations in the Netherlands: a disease in disguise. *Neth J Med, 72*(4), 210-217. Retrieved from https://www.ncbi.nlm.nih.gov/pubmed/24829177

Ducamp, S., & Fleming, M. D. (2019). The molecular genetics of sideroblastic anemia. *Blood, 133*(1), 59-69. doi:10.1182/blood-2018-08-815951

Ducamp, S., Luscieti, S., Ferrer-Cortes, X., Nicolas, G., Manceau, H., Peoc'h, K., . . . Sanchez, M. (2021). A mutation in the iron-responsive element of ALAS2 is a modifier of disease severity in a patient suffering from CLPX associated erythropoietic protoporphyria. *Haematologica, 106*(7), 2030-2033. doi:10.3324/haematol.2020.272450

Ducamp, S., Schneider-Yin, X., de Rooij, F., Clayton, J., Fratz, E. J., Rudd, A., . . . Puy, H. (2013). Molecular and functional analysis of the C-terminal region of human erythroid-specific 5-aminolevulinic synthase associated with X-linked dominant protoporphyria (XLDPP). *Hum Mol Genet, 22*(7), 1280-1288. doi:10.1093/hmg/dds531

Fang, R., Zhang, J., Yang, H., Shi, J., Zeng, H., Zhu, X., . . . Zhang, Y. (2021). Highly efficient gene editing and single cell analysis of hematopoietic stem/progenitor cells from X-linked sideroblastic anemia patients. *Signal Transduct Target Ther, 6*(1), 248. doi:10.1038/s41392-021-00622-3

Fasella, P. (1967). Pyridoxal phosphate. *Annu Rev Biochem, 36*, 185-210. doi:10.1146/annurev.bi.36.070167.001153

Ferreira, G. C. (1995). Heme biosynthesis: biochemistry, molecular biology, and relationship to disease. *J Bioenerg Biomembr, 27*(2), 147-150. doi:10.1007/BF02110029

Ferreira, G. C. (2013). Heme Synthesis. In *Encyclopedia of Biological Chemistry* (pp. 539-542).

Ferreira, G. C., & Gong, J. (1995). 5-Aminolevulinate synthase and the first step of heme biosynthesis. *J Bioenerg Biomembr, 27*(2), 151-159. doi:10.1007/BF02110030

Ferreira, G. C., Neame, P. J., & Dailey, H. A. (1993). Heme biosynthesis in mammalian systems: evidence of a Schiff base linkage between the pyridoxal 5'-phosphate cofactor and a lysine residue in 5-aminolevulinate synthase. *Protein Sci, 2*(11), 1959-1965. doi:10.1002/pro.5560021117

Ferrier, D. R. (2017). *Biochemistry* (Seventh ed.): Philadelphia: Wolters Kluwer.

Finlayson, N. D. (1990). Hereditary (primary) haemochromatosis. *BMJ, 301*(6748), 350-351. doi:10.1136/bmj.301.6748.350

Fraser, M. E., Hayakawa, K., Hume, M. S., Ryan, D. G., & Brownie, E. R. (2006). Interactions of GTP with the ATP-grasp domain of GTP-specific succinyl-CoA synthetase. *J Biol Chem, 281*(16), 11058-11065.

doi:10.1074/jbc.M511785200
Fujiwara, T., Fukuhara, N., Ichikawa, S., Kobayashi, M., Okitsu, Y., Onishi, Y., . . . Harigae, H. (2017). A novel heterozygous ALAS2 mutation in a female with macrocytic sideroblastic anemia resembling myelodysplastic syndrome with ring sideroblasts: a case report and literature review. *Ann Hematol, 96*(11), 1955-1957. doi:10.1007/s00277-017-3106-7
Furuyama, K., Fujita, H., Nagai, T., Yomogida, K., Munakata, H., Kondo, M., . . . Yamamoto, M. (1997). Pyridoxine refractory X-linked sideroblastic anemia caused by a point mutation in the erythroid 5-aminolevulinate synthase gene. *Blood, 90*(2), 822-830. Retrieved from https://www.ncbi.nlm.nih.gov/pubmed/9226183
Furuyama, K., Harigae, H., Heller, T., Hamel, B. C., Minder, E. I., Shimizu, T., . . . Sassa, S. (2006). Arg452 substitution of the erythroid-specific 5-aminolaevulinate synthase, a hot spot mutation in X-linked sideroblastic anaemia, does not itself affect enzyme activity. *Eur J Haematol, 76*(1), 33-41. doi:10.1111/j.1600-0609.2005.00541.x
Furuyama, K., & Sassa, S. (2000). Interaction between succinyl CoA synthetase and the heme-biosynthetic enzyme ALAS-E is disrupted in sideroblastic anemia. *J Clin Invest, 105*(6), 757-764. doi:10.1172/JCI6816
Gong, J., & Ferreira, G. C. (1995). Aminolevulinate synthase: functionally important residues at a glycine loop, a putative pyridoxal phosphate cofactor-binding site. *Biochemistry, 34*(5), 1678-1685. doi:10.1021/bi00005a024
Harigae, H., Furuyama, K., Kimura, A., Neriishi, K., Tahara, N., Kondo, M., . . . Sasaki, T. (1999). A novel mutation of the erythroid-specific delta-aminolaevulinate synthase gene in a patient with X-linked sideroblastic anaemia. *Br J Haematol, 106*(1), 175-177. doi:10.1046/j.1365-2141.1999.01479.x
Hariz, A., & Bhattacharya, P. T. (2024). Megaloblastic Anemia. In *StatPearls*. Treasure Island (FL) ineligible companies. Disclosure: Priyanka Bhattacharya declares no relevant financial relationships with ineligible companies.
Huang, J., & Fraser, M. E. (2022). The structure of succinyl-CoA synthetase bound to the succinyl-phosphate intermediate clarifies the catalytic mechanism of ATP-citrate lyase. *Acta Crystallogr F Struct Biol Commun, 78*(Pt 10), 363-370. doi:10.1107/S2053230X22008810
Hunter, G. A., & Ferreira, G. C. (2009). 5-aminolevulinate synthase: catalysis of the first step of heme biosynthesis. *Cell Mol Biol (Noisy-le-grand), 55*(1), 102-110. Retrieved from https://www.ncbi.nlm.nih.gov/pubmed/19268008
Hunter, G. A., & Ferreira, G. C. (2011). Molecular enzymology of 5-aminolevulinate synthase, the gatekeeper of heme biosynthesis. *Biochim Biophys Acta, 1814*(11), 1467-1473. doi:10.1016/j.bbapap.2010.12.015
Hunter, G. A., & Ferreira, G. C. (2022). An Extended C-Terminus, the Possible Culprit for Differential Regulation of 5-Aminolevulinate Synthase Isoforms. *Front Mol Biosci, 9*, 920668. doi:10.3389/fmolb.2022.920668
Jiang, M., Hong, K., Mao, Y., Ma, H., Chen, T., & Wang, Z. (2022). Natural 5-Aminolevulinic Acid: Sources, Biosynthesis, Detection and Applications. *Front Bioeng Biotechnol, 10*, 841443. doi:10.3389/fbioe.2022.841443
Kadirvel, S., Furuyama, K., Harigae, H., Kaneko, K., Tamai, Y., Ishida, Y., & Shibahara, S. (2012). The carboxyl-terminal region of erythroid-specific 5-aminolevulinate synthase acts as an intrinsic modifier for its catalytic activity and protein stability. *Exp Hematol, 40*(6), 477-486 e471. doi:10.1016/j.exphem.2012.01.013
Kaneko, K., Furuyama, K., Fujiwara, T., Kobayashi, R., Ishida, H., Harigae, H., & Shibahara, S. (2014). Identification of a novel erythroid-specific enhancer for the ALAS2 gene and its loss-of-function mutation which is associated with congenital sideroblastic anemia. *Haematologica, 99*(2), 252-261. doi:10.3324/haematol.2013.085449
Kaneko, K., Kubota, Y., Nomura, K., Hayashimoto, H., Chida, T., Yoshino, N., . . . Furuyama, K. (2018). Establishment of a cell model of X-linked sideroblastic anemia using genome editing. *Exp Hematol, 65*, 57-68 e52. doi:10.1016/j.exphem.2018.06.002
Lambeth, D. O., Tews, K. N., Adkins, S., Frohlich, D., & Milavetz, B. I. (2004). Expression of two succinyl-CoA synthetases with different nucleotide specificities in mammalian tissues. *J Biol Chem, 279*(35), 36621-36624. doi:10.1074/jbc.M406884200
Layer, G. (2020). *Comprehensive Natural Products IIIEnzymes and Enzyme Mechanisms (Radicals and Metalloenzymology)* (Third ed., Vol. 5).
Layer, G. (2021). Heme biosynthesis in prokaryotes. *Biochim Biophys Acta Mol Cell Res, 1868*(1), 118861. doi:10.1016/j.bbamcr.2020.118861
Layer, G., Reichelt, J., Jahn, D., & Heinz, D. W. (2010). Structure and function of enzymes in heme biosynthesis. *Protein Sci, 19*(6), 1137-1161. doi:10.1002/pro.405

LeBlanc, M. A., Bettle, A., Berman, J. N., Price, V. E., Pambrun, C., Yu, Z., . . . Fernandez, C. V. (2016). Study of Glycine and Folic Acid Supplementation to Ameliorate Transfusion Dependence in Congenital SLC25A38 Mutated Sideroblastic Anemia. *Pediatr Blood Cancer, 63*(7), 1307-1309. doi:10.1002/pbc.25981

Lendrihas, T., Hunter, G. A., & Ferreira, G. C. (2010). Targeting the active site gate to yield hyperactive variants of 5-aminolevulinate synthase. *J Biol Chem, 285*(18), 13704-13711. doi:10.1074/jbc.M109.074237

May, A., & Bishop, D. F. (1998). The molecular biology and pyridoxine responsiveness of X-linked sideroblastic anaemia. *Haematologica, 83*(1), 56-70. Retrieved from https://www.ncbi.nlm.nih.gov/pubmed/9542324

May, A., & Fitzsimons, E. (1994). Sideroblastic anaemia. *Baillieres Clin Haematol, 7*(4), 851-879. doi:10.1016/s0950-3536(05)80128-3

Meguro, K., Igarashi, K., Yamamoto, M., Fujita, H., & Sassa, S. (1995). The role of the erythroid-specific delta-aminolevulinate synthase gene expression in erythroid heme synthesis. *Blood, 86*(3), 940-948. Retrieved from https://www.ncbi.nlm.nih.gov/pubmed/7620186

Melefors, O., Goossen, B., Johansson, H. E., Stripecke, R., Gray, N. K., & Hentze, M. W. (1993). Translational control of 5-aminolevulinate synthase mRNA by iron-responsive elements in erythroid cells. *J Biol Chem, 268*(8), 5974-5978. Retrieved from https://www.ncbi.nlm.nih.gov/pubmed/8449958

Menotti, E., Henderson, B. R., & Kuhn, L. C. (1998). Translational regulation of mRNAs with distinct IRE sequences by iron regulatory proteins 1 and 2. *J Biol Chem, 273*(3), 1821-1824. doi:10.1074/jbc.273.3.1821

Merrill, A. H., Jr., & Henderson, J. M. (1990). Vitamin B6 metabolism by human liver. *Ann N Y Acad Sci, 585*, 110-117. doi:10.1111/j.1749-6632.1990.tb28047.x

Mollin, D. L. (1965). Sideroblasts and Sideroblastic Anaemia. *Br J Haematol, 11*, 41-48. doi:10.1111/j.1365-2141.1965.tb00082.x

Moreno-Carralero, M. I., Arrizabalaga-Amuchastegui, B., Sanchez-Calero-Guilarte, J., Morado-Arias, M., Velasco-Valdazo, A. E., de-la-Iglesia-Inigo, S., . . . Moran-Jimenez, M. J. (2019). Missense variants in ALAS2 gene in five patients. *Int J Lab Hematol, 41*(1), e5-e9. doi:10.1111/ijlh.12902

Munro, A. W., Girvan, H. M., McLean, K. J., Cheesman, M. R., & Leys, D. (2009). Heme and Hemoproteins. In *Tetrapyrroles: Birth, Life and Death* (pp. 160-183). New York, NY: Springer New York.

Nagao, T., & Hirokawa, M. (2017). Diagnosis and treatment of macrocytic anemias in adults. *J Gen Fam Med, 18*(5), 200-204. doi:10.1002/jgf2.31

Nakajima, O., Takahashi, S., Harigae, H., Furuyama, K., Hayashi, N., Sassa, S., & Yamamoto, M. (1999). Heme deficiency in erythroid lineage causes differentiation arrest and cytoplasmic iron overload. *EMBO J, 18*(22), 6282-6289. doi:10.1093/emboj/18.22.6282

Nzelu, D., Shangaris, P., Story, L., Smith, F., Piyasena, C., Alamelu, J., . . . Sankaran, S. (2021). X-linked sideroblastic anaemia in a female fetus: a case report and a literature review. *BMC Med Genomics, 14*(1), 296. doi:10.1186/s12920-021-01146-z

Ono, K., Fujiwara, T., Saito, K., Nishizawa, H., Takahashi, N., Suzuki, C., . . . Harigae, H. (2022). Congenital sideroblastic anemia model due to ALAS2 mutation is susceptible to ferroptosis. *Sci Rep, 12*(1), 9024. doi:10.1038/s41598-022-12940-9

Peoc'h, K., Nicolas, G., Schmitt, C., Mirmiran, A., Daher, R., Lefebvre, T., . . . Puy, H. (2019). Regulation and tissue-specific expression of delta-aminolevulinic acid synthases in non-syndromic sideroblastic anemias and porphyrias. *Mol Genet Metab, 128*(3), 190-197. doi:10.1016/j.ymgme.2019.01.015

Pereira, J. C., Barbot, J., & Ribeiro, M. L. (2009). Novel human pathological mutations. Gene symbol: ALAS2. Disease: sideroblastic anaemia. *Hum Genet, 126*(2), 333. Retrieved from https://www.ncbi.nlm.nih.gov/pubmed/19693999

Phillips, D., Aponte, A. M., French, S. A., Chess, D. J., & Balaban, R. S. (2009). Succinyl-CoA synthetase is a phosphate target for the activation of mitochondrial metabolism. *Biochemistry, 48*(30), 7140-7149. doi:10.1021/bi900725c

Prades, E., Chambon, C., Dailey, T. A., Dailey, H. A., Briere, J., & Grandchamp, B. (1995). A new mutation of the ALAS2 gene in a large family with X-linked sideroblastic anemia. *Hum Genet, 95*(4), 424-428. doi:10.1007/BF00208968

Rich, P. R., Marechal, A. (2012). *Comprehensive Biophysics*(Vol. 8).

Rose, C., Callebaut, I., Pascal, L., Oudin, C., Fournier, M., Gouya, L., . . . Kannengiesser, C. (2017). Lethal ALAS2 mutation in males X-linked sideroblastic anaemia. *Br J Haematol, 178*(4), 648-651. doi:10.1111/bjh.14164

Rose, C. S., Gyorgy, P., Butler, M., Andres, R., Norris, A. H., Shock, N. W., . . . Spiegel, H. (1976). Age differences in vitamin B6 status of 617 men. *Am J Clin Nutr, 29*(8), 847-853. doi:10.1093/ajcn/29.8.847

Sadlon, T. J., Dell'Oso, T., Surinya, K. H., & May, B. K. (1999). Regulation of erythroid 5-aminolevulinate

synthase expression during erythropoiesis. *Int J Biochem Cell Biol, 31*(10), 1153-1167. doi:10.1016/s1357-2725(99)00073-4
Sankaran, V. G., Ulirsch, J. C., Tchaikovskii, V., Ludwig, L. S., Wakabayashi, A., Kadirvel, S., . . . Steensma, D. P. (2015). X-linked macrocytic dyserythropoietic anemia in females with an ALAS2 mutation. *J Clin Invest, 125*(4), 1665-1669. doi:10.1172/JCI78619
Sassa, S., Akagi, R., Nishitani, C., Harigae, H., & Furuyama, K. (2002). Late-onset porphyrias: what are they? *Cell Mol Biol (Noisy-le-grand), 48*(1), 97-101. Retrieved from https://www.ncbi.nlm.nih.gov/pubmed/11929054
Schneider, S., Marles-Wright, J., Sharp, K. H., & Paoli, M. (2007). Diversity and conservation of interactions for binding heme in b-type heme proteins. *Nat Prod Rep, 24*(3), 621-630. doi:10.1039/b604186h
Scimeca, P. C., Weinblatt, M. E., & Kahn, E. (1994). Does Rapidly Progressive Iron Overload in a Young Girl with Sideroblastic Anemia Also Signify the Presence of Hereditary Hemochromatosis? *Pediatric Hematology and Oncology, 11*(1), 99-104. doi:10.3109/08880019409141906
Stojanovski, B. M., Hunter, G. A., Jahn, M., Jahn, D., & Ferreira, G. C. (2014). Unstable reaction intermediates and hysteresis during the catalytic cycle of 5-aminolevulinate synthase: implications from using pseudo and alternate substrates and a promiscuous enzyme variant. *J Biol Chem, 289*(33), 22915-22925. doi:10.1074/jbc.M114.574731
Stojanovski, B. M., Hunter, G. A., Na, I., Uversky, V. N., Jiang, R. H. Y., & Ferreira, G. C. (2019). 5-Aminolevulinate synthase catalysis: The catcher in heme biosynthesis. *Mol Genet Metab, 128*(3), 178-189. doi:10.1016/j.ymgme.2019.06.003
Taylor, J. L., Ayres-Galhardo, P. H., & Brown, B. L. (2024). Elucidating the Role of Human ALAS2 C-terminal Mutations Resulting in Loss of Function and Disease. *Biochemistry*. doi:10.1021/acs.biochem.4c00066
Taylor, J. L., & Brown, B. L. (2022). Structural basis for dysregulation of aminolevulinic acid synthase in human disease. *J Biol Chem, 298*(3), 101643. doi:10.1016/j.jbc.2022.101643
Tchaikovskii, V., Desnick, R. J., & Bishop, D. F. (2019). Molecular expression, characterization and mechanism of ALAS2 gain-of-function mutants. *Mol Med, 25*(1), 4. doi:10.1186/s10020-019-0070-9
Thomas, B., Visanica, S., Poussing, S., Gerard, D., & Perrin, J. (2023). Is this really thalassemia? *Am J Hematol*. doi:10.1002/ajh.26913
Tian, C., Zhao, J., Xiong, Q., Yu, H., & Du, H. (2023). Secondary iron overload induces chronic pancreatitis and ferroptosis of acinar cells in mice. *Int J Mol Med, 51*(1). doi:10.3892/ijmm.2022.5212
Tran, J. U., & Brown, B. L. (2023). The yeast ALA synthase C-terminus positively controls enzyme structure and function. *Protein Sci, 32*(4), e4600. doi:10.1002/pro.4600
Trefely, S., Lovell, C. D., Snyder, N. W., & Wellen, K. E. (2020). Compartmentalised acyl-CoA metabolism and roles in chromatin regulation. *Mol Metab, 38*, 100941. doi:10.1016/j.molmet.2020.01.005
Whatley, S. D., Ducamp, S., Gouya, L., Grandchamp, B., Beaumont, C., Badminton, M. N., . . . Puy, H. (2008). C-terminal deletions in the ALAS2 gene lead to gain of function and cause X-linked dominant protoporphyria without anemia or iron overload. *Am J Hum Genet, 83*(3), 408-414. doi:10.1016/j.ajhg.2008.08.003
Wintrobe, M. M., & Greer, J. P. (2004). *Wintrobe's clinical hematology* (11th ed.). Philadelphia: Lippincott Williams & Wilkins.
Wintrobe, M. M., & Greer, J. P. (2014). *Wintrobe's Clinical Hematology* (Thirteenth ed.). Philadelphia: Lippincott Williams & Wilkins.
Wolodko, W. T., Fraser, M. E., James, M. N., & Bridger, W. A. (1994). The crystal structure of succinyl-CoA synthetase from Escherichia coli at 2.5-A resolution. *J Biol Chem, 269*(14), 10883-10890. doi:10.2210/pdb1scu/pdb
Zhang, Y., Zhang, J., An, W., Wan, Y., Ma, S., Yin, J., . . . Zhu, X. (2017). Intron 1 GATA site enhances ALAS2 expression indispensably during erythroid differentiation. *Nucleic Acids Res, 45*(2), 657-671. doi:10.1093/nar/gkw901

APPENDIX A

Supplementary Information

Table AI. Additional ALAS2 XLSA Variants Generated

Residue	Mutation	Activity of Wild Type ALAS2*	Cofactor Bound (Y/N)***	Reference
Asp190	Val	1.08	Y	(Furuyama et al., 1997)
Leu313	Pro	1.08	Y	(de Gennes et al., 2022)
Ile324	Thr	N/A**	N/A	(Moreno-Carralero et al., 2019)
Gly398	Asp	0.00	N	(Astner et al., 2005)
Ser568	Gly	0.85	Y	(Harigae et al., 1999)

*Activity was determined as described previously with 300μM succinyl-CoA and 50mM glycine, 100nM protein concentration
**Severe aggregation during purification; unable to purify
***Determined with UV-Visible Spectroscopy as described

Table AII. Previously Screened Crystallization Hits

Protein	Concentration	Protein Buffer	Condition	Crystal Image	UV Image	Diffraction* (Y/N)	Resolution
ALAS2-M567I	1.0 mg/mL	100mM NaCl, 10mM Tris pH 8.2, 0.5mM TCEP	30% (v/v) 1,2-Propanediol 100 mM HEPES free acid/ Sodium hydroxide pH 7.5 20% (v/v) PEG 400	Figure AIa	Figure AIb	Y	~4 Angstroms
ALAS2-SCS (Complex)	11.0 mg/mL	100mM NaCl, 10mM Tris pH 8.2, 0.5mM TCEP	35% (v/v) 2-Ethoxyethanol 100 mM Sodium citrate/ Citric acid pH 5.5	Figure AIIa	Figure AIIb	Y	~1.9 Angstroms

*Diffraction and resolution determined using Vanderbilt's Excillum D2+ MetalJet X-ray source with PHOTON III pixel array detector

A. B.

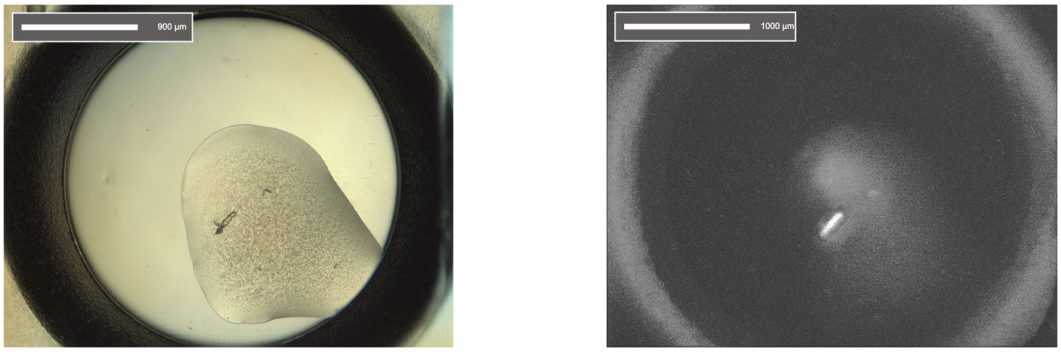

Figure AI. Image of ALAS2-M567I crystal hit (A) with associated UV image (B). Sample was prepared with 17 µM of ALAS2 M567I variant. White bar represents 900 µm scale for A and 1000 µm scale for B.

A. B.

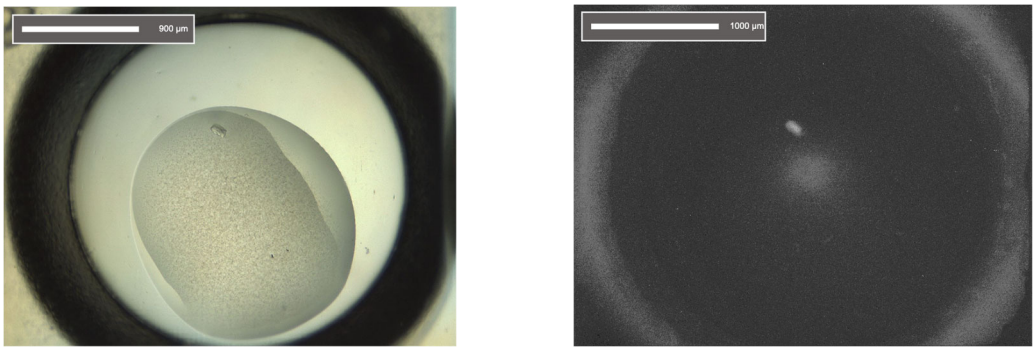

Figure AII. Image of ALAS2-SCS complex crystal hit (A) with associated UV image (B). Sample was prepared with 9 µM of ALAS2-SCS complex. White bar represents 900 µm scale for A and 1000 µm scale for B.

A.

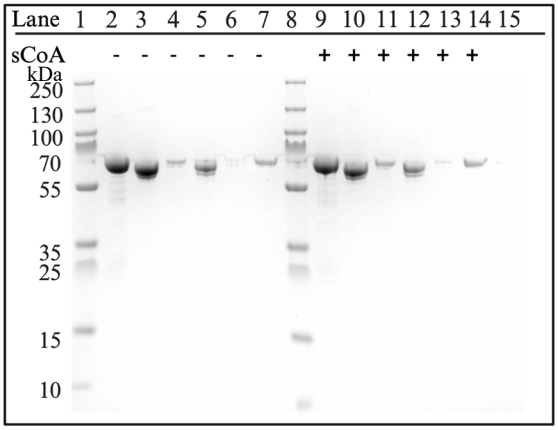

B.

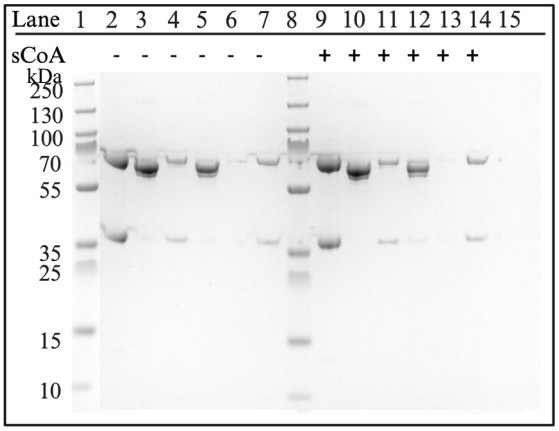

Figure AIII. SDS-PAGE analysis of His-tagged SUCLA2 (57 kDa) immobilized to NiNTA resin with ALAS2 (59 kDa) (A) or His-tagged SCS (SUCLG1 at 36 kDa and HisSUCLA2 at 57 kDa) immobilized to NiNTA resin with ALAS2 (59 kDa) (B)*. *Elution lanes are lanes 7 and 14*. (A): *Lane 1:* molecular weight marker*; lane 2:* His-SUCLA2 input (5 μM); *lane 3:* ALAS2 input (5 μM)*; lane 4:* His-SUCLA2 flow-through after NiNTA incubation*; lane 5:* ALAS2 flow-through*; lane 6:* ALAS2 final wash*; lane 7:* elution from which ALAS2 was loaded onto His-SUCLA2 bound resin*; lane 8:* molecular weight marker; *lane 9*: His-SUCLA2 input (5 μM) with succinyl-CoA; *lane 10*: ALAS2 input (5 μM) with succinyl-CoA*; lane 11:* His-SUCLA2 flow-through after NiNTA incubation with succinyl-CoA*; lane 12:* ALAS2 flow-through with succinyl-CoA; *lane 13*: ALAS2 final wash with succinyl-CoA*; lane 14:* elution from which ALAS2 was loaded onto His-SUCLA2 bound resin with succinyl-CoA. (B): *Lane 1:* molecular weight marker*; lane 2:* His-SCS input (5 μM) with SUCLG1 at 36 kDa and His-SUCLA2 at 57 kDa; *lane 3:* ALAS2 input (5 μM*; lane 4:* His-SCS flow-through after NiNTA incubation*; lane 5:* ALAS2 flow-through*; lane 6:* ALAS2 final wash*; lane 7:* elution from which ALAS2 was loaded onto His-SCS bound resin*; lane 8:* molecular weight marker; *lane 9*: His-SCS input (5 μM) with SUCLG1 at 36 kDa and His-SUCLA2 at 57 kDa with succinyl-CoA; *lane 10*: ALAS2 input (5 μM) with succinyl-CoA*; lane 11:* His-SCS flow-through after NiNTA incubation with succinyl-CoA*; lane 12:* ALAS2 flow-through with succinyl-CoA; *lane 13*: ALAS2 final wash with succinyl-CoA*; lane 14:* elution from which ALAS2 was loaded onto His-SCS bound resin with succinyl-CoA.

*"sCoA" indicates the addition or omission of succinyl-CoA